Meshes with Spherical Faces

MARTIN KILIAN, TU Wien, Austria
ANTHONY S RAMOS CISNEROS, KAUST, Saudi Arabia
CHRISTIAN MÜLLER, TU Wien, Austria
HELMUT POTTMANN, KAUST, Saudi Arabia

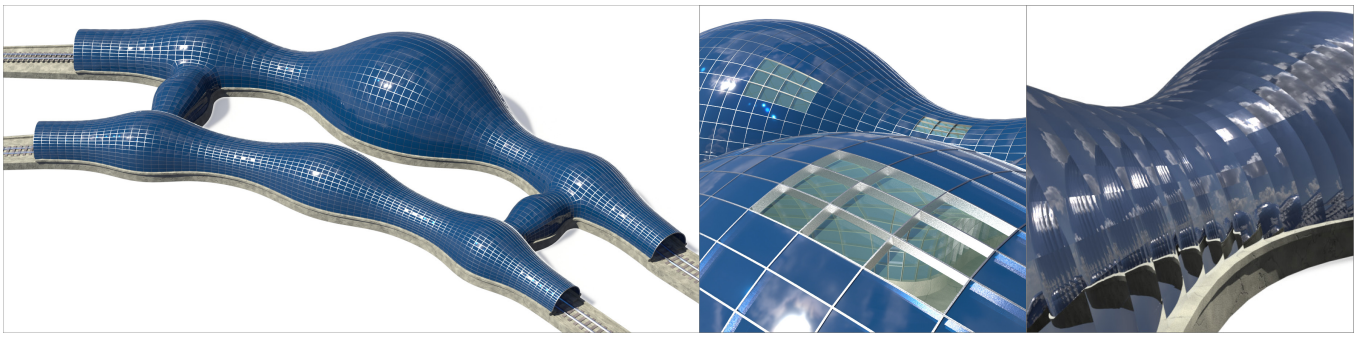

Fig. 1. An abstract roof structure that we put into the context of a hypothetical train station. We replaced all faces of the given circular PQ-mesh by spherical surface patches (*left*). The minimization of intersection angles of neighboring spheres produces a smooth appearance where the surface is positively curved and a mild strip pattern in negatively curved regions (*right*). Furthermore, we optimized the sphere mesh for the existence of a geometric support structure, consisting of annuli (*center*) which can be used to mount panels. Four annuli around a vertex intersect each other along a common axis.

Discrete surfaces with spherical faces are interesting from a simplified manufacturing viewpoint when compared to other double curved face shapes. Furthermore, by the nature of their definition they are also appealing from the theoretical side leading to a Möbius invariant discrete surface theory. We therefore systematically describe so called sphere meshes with spherical faces and circular arcs as edges where the Möbius transformation group acts on all of its elements. Driven by aspects important for manufacturing, we provide the means to cluster spherical panels by their radii. We investigate the generation of sphere meshes which allow for a geometric support structure and characterize all such meshes with triangular combinatorics in terms of non-Euclidean geometries. We generate sphere meshes with hexagonal combinatorics by intersecting tangential spheres of a reference surface and let them evolve – guided by the surface curvature – to visually convex hexagons, even in negatively curved areas. Furthermore, we extend meshes with circular faces of all combinatorics to sphere meshes by filling its circles with suitable spherical caps and provide a remeshing scheme to obtain quadrilateral sphere meshes with support structure from given sphere congruences. By broadening polyhedral meshes to sphere meshes we exploit the additional degrees of freedom to minimize intersection angles of neighboring spheres enabling the use of spherical panels that provide a softer perception of the overall surface.

CCS Concepts: • **Computing methodologies** → **Shape modeling**.

Additional Key Words and Phrases: discrete differential geometry, architectural geometry, computational design, sphere geometry, sphere mesh, spherical paneling

ACM Reference Format:
Martin Kilian, Anthony S Ramos Cisneros, Christian Müller, and Helmut Pottmann. 2023. Meshes with Spherical Faces. *ACM Trans. Graph.* 42, 6, Article 184 (December 2023), 19 pages. https://doi.org/10.1145/3618345

1 INTRODUCTION

The manufacturing process of freeform surface patches as façades, roofs, or in any other architectural context, heavily depends on the scale, used materials, carrying loads, and many other aspects. An overall smooth appearance of the visual surface skin is often a design goal. To reach this goal, the freeform surface becomes segmented into panels of manufacturable size. The segmentation, or better the mesh resulting from the segments, can be part of the design. In architectural designs the mesh is therefore quite often present before a geometry-aware segmentation process could produce simpler panel shapes. Also crucial for a smooth appearance of the fabricated surface is the use of doubly curved panels, e.g., double curved glass, or metal sheets. Even though a smart design with planar panels can improve visual appearance [Pellis et al. 2019], doubly curved panels are unavoidable for perfect smoothness. However, since the manufacturing of doubly curved panels requires the fabrication of

Authors' addresses: Martin Kilian, martin.kilian@tuwien.ac.at, Inst. of Discr. Math. and Geometry, TU Wien, Austria; Anthony S Ramos Cisneros, anthony.cisneros@kaust.edu.sa, Computer, Electrical and Mathematical Sciences and Engineering Division, KAUST, Saudi Arabia; Christian Müller, christian.mueller@tuwien.ac.at, Inst. of Discr. Math. and Geometry, TU Wien, Austria; Helmut Pottmann, helmut.pottmann@kaust.edu.sa, Computer, Electrical and Mathematical Sciences and Engineering Division, KAUST, Saudi Arabia.

0730-0301/2023/12-ART184 $15.00
https://doi.org/10.1145/3618345

Fig. 2. Spherical glass panels are used by the *Nur Alem Museum of Future Energy* in Astana, Kazakhstan.

a mold per panel, this easily exceeds the available budget. Depending on the material, like glass, for example, an additional uniquely produced transport packaging form often needs to be made too.

Optimizing for repetitive shapes or potential mold re-use is a good strategy to balance between production costs and aesthetic design goals. Mold re-use or clustering panel types is an active research topic [Eigensatz et al. 2010; Pellis et al. 2021; Wang et al. 2019].

The present paper contributes to the balancing of using double curved panels and mold re-use by restricting to a panel type with a very large symmetry group, namely spheres. We provide approximation and modeling methods, remeshing, and clustering strategies to obtain *meshes with spherical faces* and *circular arcs as edges*. The practicability of our paper is affirmed by the availability of machines to produce spherical panels. See Fig. 2 for a recent building.

This topic belongs to the Möbius geometry of spheres. While the few existing discrete surface theories in Möbius geometry are usually only invariant under Möbius transformations applied to vertices or spheres, a systematic study of sphere meshes is missing. Our novel approach treats the entire *sphere mesh* (i.e., including edges and faces) as a truly *Möbius invariant* object.

Not every mathematically computed geometric shape/mesh can be realized as a stable building. Thus we also study and optimize for viable and geometry-aware *support structures*. The visual smoothness of *intersection angle minimizing* sphere meshes provides a designer with a tool to create surfaces with a very soft and smoothly pleasing appeal (see, e.g., Figure 3). For that we approximate given surfaces with sphere meshes.

It turns out that sphere meshes with *different combinatorics* should be treated differently even though there are overlaps between the settings. Throughout the paper we denote sphere meshes with triangle combinatorics, i.e., where the faces are spherical patches with circular boundaries, by *STriangle-meshes*, those with quad combinatorics by *SQ-meshes*, and those with hexagonal faces *SHex-meshes*.

1.1 Overview and contributions

The goal of the present paper is the start of a systematic study of truly Möbius invariant sphere meshes. After a discussion of the related work we provide the necessary concepts and notions of sphere geometry. In particular, the central sphere as well as smooth and discrete sphere congruences take up substantial space in Section 2.

- We discuss general properties that are involved in paneling with spherical faces such as *minimizing the intersection angles* of neighboring spherical faces (Sec. 4.2). This is particularly interesting for circular meshes where we can choose from a one-parameter family of spheres per face.
- The existence of a geometry-aware *support structure* of spherical meshes is not for free. We characterize all sphere meshes which allow for a geometric support structure in Section 4.1 and provide a strategy to optimize for it.
- Especially useful for mold re-use of spherical panels is *clustering* them by equal radii which we deal with in Section 4.3.
- Triangular sphere meshes (STriangle-mesh) automatically fall into three types. This leads to a simple way of transforming conventional triangle meshes into STriangle-meshes (Section 5).
- Quadrilateral sphere meshes (SQ-meshes) whose edges follow discrete principal directions and allow for a *discrete central sphere congruence* (Sec. 6.1) which in itself is almost an *angle minimizing* SQ-mesh (Sec. 6.2). Our method to minimize intersection angles is not restricted to quad combinatorics (see, e.g., Figure 3).
- Some sphere congruences (not all) can be *remeshed* into an SQ-mesh with support structure. We introduce a scheme including a novel remeshing idea in the space of spheres to transform existing sphere meshes into SQ-meshes with support structure in Sec. 6.4.
- We intersect tangential spheres that must be chosen in a sensible way (details in Sec. 7) to generate *SHex-meshes* approximating a reference surface (Sec. 7). A nice feature is that we can choose spheres such that even negatively curved surface regions can be paneled by visually convex spherical faces (Figure 32).

1.2 Organisation of the paper — road map

The most important objects in this paper are spheres. We start in Section 2 with representing them and provide the tools necessary to study sphere meshes. We continue with a brief description of the numerical algorithm for our optimization part (Sec. 3). It is about minimizing an energy consisting of several energy terms that enforce specific properties of sphere meshes. We will present the definition of each energy term in the subsequent sections where we introduce the respective geometric property. In Section 4 we introduce the paneling problem with spherical panels and declare what we mean by the existence of a geometric support structure. We talk about general properties of sphere meshes like angle minimizing panels, clustering of face spheres by their radii, and introduce energies for increasing the quality of the support structure.

It turns out that the combinatorics of a sphere mesh has a significant influence on the existence of a support structure and some other properties. We therefore discuss triangular, quadrilateral and

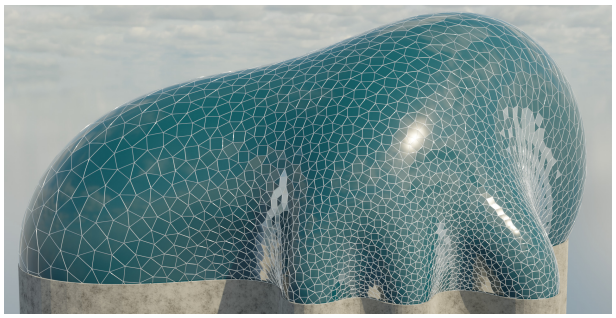

Fig. 3. A mesh with semi regular combinatorics and spherical faces.

hexagonal sphere meshes in separate sections (Sec. 5, 6, 7). We end the paper with a short conclusion and discussion about limitations and future work (Sec. 8).

1.3 Related work

Discrete and computational geometry. The alpha-shapes of [Edelsbrunner and Mücke 1994] are a generalization of the convex hull of a point set using spheres and gave rise to a series of contributions in discrete and computational geometry that involve spheres in their construction. As this is not closely related to our work, we just point to fundamentals on the union of balls [Edelsbrunner 1993], their use to describe deformable surfaces and molecular skins [Cheng and Shi 2005; Cheng et al. 2001; Edelsbrunner 1999] and their role in computational topology [Edelsbrunner and Harer 2010].

Sphere geometries in classical and discrete differential geometry. A mesh with spherical faces is a discrete version of a two-parameter family of spheres, a so-called sphere congruence, whose differential geometric theory within the classical sphere geometries is found in the monographs by Blaschke [1929] and Hertrich-Jeromin [2003]. There is much less research in the discrete setting. Most contributions deal with principal curvature parameterizations, triply orthogonal surface systems and the closely related Ribaucour congruences [Bobenko and Suris 2006; Bobenko and Suris 2007; Bobenko and Suris 2008; Rörig and Szewieczek 2021].

A sphere geometric approach to the smooth extension of principal nets by Dupin cyclide patches is found in [Bobenko and Huhnen-Venedey 2012]; for a computational approach and applications in architecture we also refer to the circular arc structures of [Bo et al. 2011]. Surface parameterizations whose parameter lines are symmetric with respect to the principal directions are sphere geometric objects, and discrete versions of them have been proposed for applications in architecture and CNC machining [Pellis et al. 2020].

Geometry processing. Bobenko and Schröder [2005] developed an elegant Möbius geometric formulation of the Willmore energy based on triangle meshes and applied it to the modeling of fair surfaces. For a recent stable and efficient computational approach to the Willmore flow and constrained Willmore surfaces we refer to [Crane et al. 2013; Soliman et al. 2021].

Meshes whose vertices are spheres rather than points constitute a medial representation of shapes, with applications to shape approximation and deformation, real-time hand modeling and tracking [Thiery et al. 2013, 2016; Tkach et al. 2016]. Spheres appear as local approximations within the generation of surfaces from point clouds [Guennebaud and Gross 2007] and in recent work on design rationalization [Jadon et al. 2022]. A one-dimensional angle optimization approach by replacing straight edges in planar combinatorial graphs by circular arcs has been studied in [Aichholzer et al. 2015]. We also point to surface deformation using Möbius transformations [Vaxman et al. 2015] and Möbius invariant subdivision schemes [Vaxman et al. 2018].

Paneling architectural surfaces. Paneling freeform surfaces is a major task in Architectural Geometry [Pottmann et al. 2015]. Eigensatz et al. [2010] presented a computational solution that provides a user-guided trade-off between cost of fabrication and quality of the final skin. Recent work on paneling addressed the visual smoothness achievable with flat panels [Pellis et al. 2019], the effective use of panels of constant Gaussian curvature when working with materials that can still be bent after being formed over a mold [Jiang et al. 2021] and the advantage of slightly modifying a design surface towards a Weingarten surface [Pellis et al. 2021]. Spherical panels of constant radius have been suggested for paneling a special class of surfaces, the hyperbolic linear Weingarten surfaces [Liu et al. 2023].

2 GEOMETRY OF SPHERES AND ENVELOPES OF SPHERE FAMILIES

In this section we introduce basic notions of sphere geometry that are important in our paper. In particular we present a practical notion of intersection angle between spheres, the point model of Möbius geometry, sphere pencils, sphere congruences and their envelopes. We discuss several parametrizations and classes of sphere congruences and their discretizations with the view towards approximating and generating freeform surface skins. The central type of geometry which is important at many places throughout the paper is Möbius geometry with its objects, notions and properties. Let us start with quickly setting the scene.

Möbius geometry. A *Möbius transformation* is a bijective map $m : \mathbb{R}^3 \cup \infty \to \mathbb{R}^3 \cup \infty$ which maps spheres and planes to spheres and planes (possibly swapping between them), where ∞ denotes a single point at infinity. A plane is considered as a sphere with infinite radius and passing through ∞. *Möbius geometry* studies objects, notions and properties that stay invariant under Möbius transformations. Such objects, notions and properties are therefore called *Möbius invariant* and will appear throughout the paper.

2.1 Representations of spheres

We declare basic notations starting with expressing a sphere through the coefficients of its equation and then considering point models for spheres by virtue of the stereographic projection. We express intersection angles and sphere pencils in terms of these models.

Sphere equation. Any sphere or plane in $\mathbb{R}^3$ can be expressed as set of points $\mathbf{x} = (x, y, z)$ fulfilling an equation of the form

$$A(x^2 + y^2 + z^2) - B_1 x - B_2 y - B_3 z + C = 0,$$

with $A, B_1, B_2, B_3, C \in \mathbb{R}$, or simply

$$A\mathbf{x}^2 - \langle B, \mathbf{x} \rangle + C = 0, \tag{1}$$

where $B = (B_1, B_2, B_3)$ and $\langle \cdot, \cdot \rangle$ denotes the Euclidean scalar product. If $A = 0$ then Equation (1) represents a plane with normal vector B and distance $C/\|B\|$ to the origin. If $A \neq 0$ then Equation (1) represents a sphere with center $\frac{B}{2A}$ and radius $\sqrt{\frac{\|B\|^2 - 4AC}{4A^2}}$. The radius can be imaginary, in which case Equation (1) represents an imaginary sphere (i.e., a sphere with negative squared radius). In the case of a real sphere where we have $\|B\|^2 - 4AC > 0$, Equation (1) can be multiplied with a real number such that its coefficients "normalize" to $\|B\|^2 - 4AC = 1$.

Stereographic projection and point model of Möbius geometry. The *stereographic projection* of a point $\mathbf{x} \in \mathbb{R}^3$ is its central projection

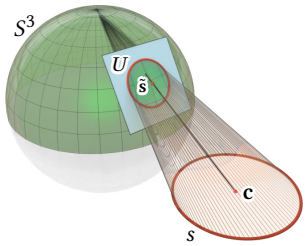

Fig. 4. Schematic illustration (one dimension lower) of the stereographic projection of a two-dim. sphere s in $\mathbb{R}^3$ to the three-dim. sphere S^3 in $\mathbb{R}^4$. The three-dim. affine subspace U intersects S^3 in the stereographic projection of s. The pole of U is the point $\tilde{\mathbf{s}}$ which is projected to the center $\mathbf{c}$ of s by the central projection from the north pole.

with the north pole $(0,0,0,1)$ as center to the three-dimensional sphere $S^3 \subset \mathbb{R}^4$ and reads

$$\mathbf{x} \longmapsto \left(\frac{2\mathbf{x}}{\mathbf{x}^2+1}, \frac{\mathbf{x}^2-1}{\mathbf{x}^2+1}\right) \in S^3.$$

The same stereographic projection maps a 2D sphere s with center $\mathbf{c} \in \mathbb{R}^3$ and radius r to a 2D sphere contained in the intersection of a three-dimensional affine subspace U with the three-dimensional sphere S^3. See Figure 4 for an illustration (one dimension lower). The pole of U with respect to S^3 equals

$$\tilde{\mathbf{s}} := \left(\frac{2\mathbf{c}}{\mathbf{c}^2-r^2+1}, \frac{\mathbf{c}^2-r^2-1}{\mathbf{c}^2-r^2+1}\right) \in \mathbb{R}^4. \tag{2}$$

The central projection of $\tilde{\mathbf{s}}$ from the north pole to $\mathbb{R}^3$ yields the center $\mathbf{c}$ of the sphere s. Note that formula (2) only makes sense if the denominator $\mathbf{c}^2-r^2+1$ does not vanish. For spheres with $\mathbf{c}^2-r^2+1 = 0$ the pole is a point at infinity. We therefore projectively extend $\mathbb{R}^4$ by adding points at infinity to become the four-dimensional projective space:

$$\begin{aligned} \mathbb{R}^4 &\longrightarrow P^4 = \{[\mathbf{x}] \subset \mathbb{R}^5 \mid \mathbf{x} \in \mathbb{R}^5, \mathbf{x} \neq 0\} \\ (x_1,\dots,x_4) &\longmapsto [x_1,\dots,x_4,1] \end{aligned}$$

where $[\cdot]$ denotes the linear span. Consequently, spheres and planes in $\mathbb{R}^3$ correspond to points in P^4 which form the *point model of Möbius geometry*. In this model the spheres are represented by

$$[(\tilde{\mathbf{s}},1)] = [(2\mathbf{c}, \mathbf{c}^2-r^2-1, \mathbf{c}^2-r^2+1)] = [(B, C-A, C+A)].$$

Any vector spanning this one-dimensional subspace is referred to as *pentaspherical coordinates* which are only determined up to a common multiple. We choose

$$\hat{\mathbf{s}} := (2\mathbf{c}, \mathbf{c}^2-r^2-1, \mathbf{c}^2-r^2+1) \in \mathbb{R}^5$$

as our "standard lift" of a sphere s with center $\mathbf{c}$ and radius r to the space of homogeneous coordinates. A point $\mathbf{p} \in \mathbb{R}^3$ – which can be seen as a sphere with radius 0 – is therefore lifted to

$$\hat{\mathbf{p}} := (2\mathbf{p}, \mathbf{p}^2-1, \mathbf{p}^2+1) \in \mathbb{R}^5,$$

and a plane τ with equation $\langle \mathbf{x}, \mathbf{n}\rangle = d$ with unit normal vector $\mathbf{n}$ is lifted to

$$\hat{\tau} := (\mathbf{n}, d, d) \in \mathbb{R}^5.$$

Viewing $\mathbb{R}^5$ as Minkowski space $(\mathbb{R}^{4,1}, \langle\!\langle\cdot,\cdot\rangle\!\rangle)$ with the inner product $\langle\!\langle\cdot,\cdot\rangle\!\rangle$ with signature $(+\,+\,+\,+\,-)$, we have $\langle\!\langle \hat{\mathbf{p}}, \hat{\mathbf{p}}\rangle\!\rangle = 0$ which expresses that $\hat{\mathbf{p}}$ lies on the sphere S^3 with equation $\langle\!\langle \mathbf{x}, \mathbf{x}\rangle\!\rangle = 0$. Since also $\langle\!\langle \hat{\mathbf{s}}, \hat{\mathbf{p}}\rangle\!\rangle = 2(r^2 - \|\mathbf{c}-\mathbf{p}\|^2)$ we conclude that a point $\mathbf{p}$ lies on a sphere s if and only if

$$\langle\!\langle \hat{\mathbf{s}}, \hat{\mathbf{p}}\rangle\!\rangle = 0, \tag{3}$$

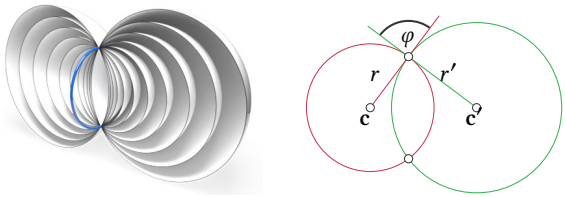

Fig. 5. *Left:* An elliptic sphere pencil: all spheres passing through a real circle. *Right:* The law of cosines yields for the intersection angle φ between the two circles or spheres to fulfill $\|\mathbf{c}-\mathbf{c}'\|^2 = r^2 + r'^2 - 2rr'\cos\varphi$.

and similarly a point $\mathbf{p}$ lies on a plane τ if and only if $\langle\!\langle \hat{\tau}, \hat{\mathbf{p}}\rangle\!\rangle = 0$. The set of all spheres passing through a point $\mathbf{p}$ is represented in P^4 by the three-dimensional polar hyperplane $\hat{\mathbf{p}}^\perp$ given by the equation $\langle\!\langle \hat{\mathbf{p}}, \mathbf{x}\rangle\!\rangle = 0$.

Sphere pencils. Any two different spheres

$$s\colon A\mathbf{x}^2 - \langle B, \mathbf{x}\rangle + C = 0 \quad \text{and} \quad s'\colon A'\mathbf{x}^2 - \langle B', \mathbf{x}\rangle + C' = 0, \tag{4}$$

intersect in a circle k which can be real or imaginary, or which can degenerate to just a point. All points of this circle k satisfy both equations (4) and therefore all linear combinations thereof:

$$(\lambda A + \mu A')\mathbf{x}^2 - \langle \lambda B + \mu B', \mathbf{x}\rangle + \lambda C + \mu C' = 0.$$

This equation represents for all homogeneous parameters $(\lambda,\mu) \neq 0$ all spheres of the *sphere pencil* spanned by the circle k (see Figure 5 left). If the intersection of all spheres of the pencil is a real circle, [an imaginary circle, or a point] the pencil is called *elliptic*, [*hyperbolic*, or *parabolic*]. Sphere pencils spanned by two spheres s, s' therefore correspond in the point model P^4 to straight lines parametrized in homogeneous coordinates by $\lambda\hat{s} + \mu\hat{s}'$.

Intersection angles. The law of cosines implies that the intersection angle φ of two spheres s, s' obeys $\|\mathbf{c}-\mathbf{c}'\|^2 = r^2+r'^2-2rr'\cos\varphi$ (see Fig. 5 right). A simple computation shows that the intersection angle can be computed in terms of the Minkowski inner product as

$$\cos\varphi = \frac{\langle\!\langle \hat{\mathbf{s}}, \hat{\mathbf{s}}'\rangle\!\rangle}{\sqrt{\langle\!\langle \hat{\mathbf{s}}, \hat{\mathbf{s}}\rangle\!\rangle}\sqrt{\langle\!\langle \hat{\mathbf{s}}', \hat{\mathbf{s}}'\rangle\!\rangle}},$$

(cf. [Bobenko and Suris 2008, p. 348]). With the notions of Equation (1) with normalized coefficients the intersection angle satisfies

$$\operatorname{sign}(AA')\cos\varphi = \langle B, B'\rangle - 2(A'C + AC'), \tag{5}$$

as follows again from rearranging terms. Consequently, two spheres s, s' are orthogonal if and only if $\langle\!\langle \hat{\mathbf{s}}, \hat{\mathbf{s}}'\rangle\!\rangle = 0$ or they are in tangential contact if and only if $|\langle\!\langle \hat{\mathbf{s}}, \hat{\mathbf{s}}'\rangle\!\rangle| = \sqrt{\langle\!\langle \hat{\mathbf{s}}, \hat{\mathbf{s}}\rangle\!\rangle}\sqrt{\langle\!\langle \hat{\mathbf{s}}', \hat{\mathbf{s}}'\rangle\!\rangle}$. Therefore, in analogy to the set of all spheres passing through a point $\mathbf{p}$ (expressed by Equation (3)), the set of all spheres orthogonal to a given sphere ω is represented in P^4 by the three-dimensional polar hyperplane $\hat{\omega}^\perp$ with equation $\langle\!\langle \hat{\omega}, \mathbf{x}\rangle\!\rangle = 0$.

2.2 Sphere congruences and envelopes of spheres

The classical case of a *sphere congruence* is a two parameter family of spheres or planes in $\mathbb{R}^3$ [Eisenhart 1962, p. 238]. With the terminology of Sec. 2.1 a sphere congruence is a two-dimensional surface $\hat{\mathbf{s}}(u,v)$ in P^4. We will only consider regular sphere congruences

where the surfaces traced out by the centers is regularly parametrized, i.e., where $\mathbf{c}_u, \mathbf{c}_v$ are linearly independent. Note that not all surfaces $\hat{\mathbf{s}}(u,v) \in P^4$ represent sphere congruences with real spheres and not all sphere congruences envelope real surfaces. In the following we will discuss several classes and parametrizations of sphere congruences which are important for us.

A sphere congruence where one family of spheres is constant, i.e., a one-parameter family of spheres, generically envelopes a *canal surface* [Blaschke and Leichtweiß 1973, p. 188]. This is an important surface class, but we exclude it due to our regularity requirement.

2.2.1 General sphere congruence. Let us denote the equation of the spheres with centers $\mathbf{c}(u,v)$ and radii $r(u,v)$ by

$$s(u,v,\mathbf{x}) := \|\mathbf{x}-\mathbf{c}\|^2 - r^2 = 0.$$

The elementary method to find the envelope of a two-parameter family of implicitly given surfaces amounts to computing the set of points fulfilling the surface equation and its two partial derivatives (see e.g. [Pottmann and Peternell 2000]). In our case, where the surfaces are spheres with equation $s(u,v,\mathbf{x}) = 0$, the enveloping points at parameters (u,v) are obtained by solving the three equations

$$s(u,v,\mathbf{x}) = 0, \quad \partial_u s(u,v,\mathbf{x}) = 0, \quad \partial_v s(u,v,\mathbf{x}) = 0.$$

The first equation represents the sphere at (u,v), while the second and third equation represent planes:

$$\langle \mathbf{x}-\mathbf{c}, \mathbf{c}_u\rangle + r r_u = 0, \quad \langle \mathbf{x}-\mathbf{c}, \mathbf{c}_v\rangle + r r_v = 0.$$

Note that the intersection of these three surfaces might not be real for all (u,v) in which case there is no real envelope. The following lemma provides a criterion for the existence of real envelopes which we prove in the appendix (Sec. A.1).

Lemma 2.1. *A congruence of spheres with centers $\mathbf{c}(u,v)$ and radii $r(u,v)$ has two real envelopes if and only if*

$$\|\mathbf{c}_u\|^2\|\mathbf{c}_v\|^2 - \langle \mathbf{c}_u, \mathbf{c}_v\rangle^2 > \|r_u\mathbf{c}_v - r_v\mathbf{c}_u\|^2.$$

We denote the two envelopes by $\mathbf{f}^+(u,v)$ and $\mathbf{f}^-(u,v)$, see Fig. 6.

Conjugate parametrization. We need the notion of conjugate directions throughout our paper (cf. [Bobenko and Suris 2008, p. 2]).

Definition 2.2. *Let $\mathbf{f}: \mathbb{R}^2 \to \mathbb{R}^n$ be a surface parametrization. Two directions $\mathbf{t}, \bar{\mathbf{t}} \in \mathbb{R}^2$ in the parameter domain describe* conjugate *directions if they are orthogonal with respect to the second fundamental form, i.e., $\mathbf{t} \cdot \mathrm{II} \cdot \bar{\mathbf{t}} = 0$. The parametrization $\mathbf{f}$ is called* conjugate *if in all points its two tangent directions are conjugate.*

Equivalently, $\mathbf{f}$ is conjugate if there are functions a, b such that $\mathbf{f}_{uv} = a\mathbf{f}_u + b\mathbf{f}_v$ or $\mathbf{f}_{uv} \in [\mathbf{f}_u, \mathbf{f}_v]$. In terms of a projective map $\hat{\mathbf{f}}: \mathbb{R}^2 \to P^n$ conjugate means $\mathbf{f}_{uv} \in [\hat{\mathbf{f}}, \hat{\mathbf{f}}_u, \hat{\mathbf{f}}_v]$.

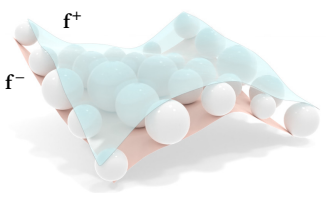

Fig. 6. Sphere congruences are two parameter families of spheres. In this example the sphere congruence (illustrated by a sparse sampling of the two parameter family of spheres) has two envelopes $\mathbf{f}^+$ and $\mathbf{f}^-$.

2.2.2 Principal parametrization. Any sphere congruence can be parametrized in such a way that the lift $\hat{\mathbf{s}}$ is a conjugate parametrization (see, e.g., [Bobenko and Suris 2008, p. 19]). It is then called a *principal parametrization*. However this property only holds over the complex numbers and not necessarily over the reals, meaning that the conjugate parametrization might not be real. If it is real, the centers $\mathbf{c}$ form also a conjugate parametrization (see [Bobenko and Suris 2008, Th. 1.22]) which has important consequences for applications (see Section 4.1).

2.2.3 Ribaucour sphere congruence. A sphere congruence is called *Ribaucour sphere congruence* if the curvature lines on $\mathbf{f}^+$ and $\mathbf{f}^-$ correspond to each other via touching spheres in the congruence. This is a special principally parametrized sphere congruence. Consequently, the centers $\mathbf{c}$ of the spheres of a Ribaucour sphere congruence generate a *conjugate net*. Furthermore, for each parameter (u,v) there exist two orthogonally intersecting circles which are in tangential contact with the two pairs of corresponding tangents of the principal curvature lines. Note that if one of the two envelopes, $\mathbf{f}^+$ or $\mathbf{f}^-$, is a sphere or plane then this sphere congruence is automatically Ribaucour (since all curves on a sphere or plane are curvature lines).

2.2.4 Principal curvature sphere congruences. Any surface $\mathbf{f}$ in $\mathbb{R}^3$ with unit normal vector field $\mathbf{n}$ and with principal curvatures κ_1, κ_2 gives rise to two *principal curvature sphere congruences* with centers $\mathbf{f} + \frac{1}{\kappa_i}\mathbf{n}$ and radii $\frac{1}{|\kappa_i|}$. They are not to be confused with "principally parametrized sphere congruences" as considered above. The principal curvature sphere congruences are the only ones which envelope exactly one surface instead of two [Blaschke 1929, p. 343].

2.2.5 Central sphere congruence. The principal spheres, their contact point on the surface $\mathbf{f}$ and its tangent plane belong to the same parabolic sphere pencil. Its spheres can be oriented by assigning a signed radius depending on which side of the tangent plane they lie. Note that this orientation is *not* Möbius invariant. Now the *central sphere* or *mean curvature sphere* is that sphere of the parabolic pencil which has signed radius $1/H$ where $H = \frac{1}{2}(\kappa_1 + \kappa_2)$ denotes the mean curvature [Blaschke 1929]. In this way the central sphere represents the average curvature in a surface point. The central sphere is Möbius invariant even though neither the mean curvature nor the signs of the principal spheres s, s' or the principal curvatures are Möbius invariant. The Möbius invariance of the central sphere s_z follows immediately from its equivalent characterization via the cross-ratio $\mathrm{cr}(\hat{\mathbf{s}}_{\kappa_1}, \hat{\mathbf{f}}, \hat{\mathbf{s}}_{\kappa_2}, \hat{\mathbf{s}}_z) = -1$ (cf. [Blaschke 1929, p. 298]).

We will utilize the *central sphere congruence*, or discretizations thereof, as initial guess for a discrete family of spheres approximating a given surface (Sec. 4).

2.3 Sphere meshes and discrete sphere congruences

Discrete surfaces are often understood as meshes that are "locally" cell decompositions of a disc. If all faces of such a mesh are planar we refer to it as *polyhedral* surfaces. In our paper we generalize this notion by allowing spherical faces to replace the planar faces. Such *sphere meshes* are combinatorially the same as conventional meshes but with spherical faces and circular arcs as edges. Planar faces are still allowed as we consider planes as spheres with infinite radius. Consequently, it makes sense to talk about STriangle-, SQ-,

or SHex-meshes depending on the combinatorics. Each face of a sphere mesh defines a sphere which we call *face sphere*. All such face spheres of a sphere mesh define a discrete family of spheres which, considered in the space of spheres P^4, generate a mesh with dual combinatorics (a vertex of the mesh in P^4 representing a face sphere). This leads us to the following definition.

Definition 2.3. *A* discrete sphere congruence *is a family of spheres each corresponding to a vertex of a combinatorial mesh understood as a cell decomposition of a two-dimensional manifold.*

Note that if a sphere congruence corresponds to a sphere mesh (we will make that connection clearer below) their combinatorics are dual to each other. Discrete sphere congruences also appear in mathematical research (see e.g., [Bobenko and Suris 2008; Rörig and Szewieczek 2021]). In the case of $\mathbb{Z}^2$ combinatorics it is natural to consider the sphere mesh or the discrete sphere congruence as *discretely parametrized* with coordinate directions.

2.3.1 General discrete sphere congruence. We can impose several geometric properties upon a discrete sphere congruence which we will specify in the following sections. Without any additional specified requirements we refer to a discrete sphere congruence as *general*. In that case, edge-neighboring spheres can intersect each other or be contained in each other or can lie outside of each other. However, in particular with the view towards applications (e.g., architectural freeform skins) it is sensible to ask for edge-neighboring spheres to intersect each other along real circles (as a minimal requirement to make the surface skin "waterproof"). Here we are only interested in congruences that define an envelope:

Definition 2.4. *We say that a discrete sphere congruence* envelopes a sphere mesh *if the spheres corresponding to a combinatorial face intersect each other in a point, the* discrete contact point.

This discrete definition is motivated by the simple imagination used in many – often older – differential geometry books to justify that an envelope is the limit of the intersection of (infinitesimally) close elements of a family of surfaces. This idea would fail if neighboring elements do not intersect at all. Like, for example, the curvature circles of a planar curve with strictly monotonically increasing curvature do not intersect at all no matter how close they are. However, with our applications in mind we will neglect such special cases and still require discrete neighboring elements (in our case spheres) to intersect to form an envelope. Note that the combinatorics of an *enveloping mesh* is by definition dual to the combinatorics of the underlying sphere congruence.

The case where the spheres of a combinatorial face intersect in two points yields two enveloping meshes and is treated later in connection with support structures (Sec. 4.1). If the spheres intersect in two points, their centers must lie in their symmetry plane (see Figure 7 left). A special instance of that is the *Q-congruence of spheres* [Bobenko and Suris 2008, p. 110], a discrete analogue of a principally parametrized sphere congruence. It is a discrete sphere congruence with $\mathbb{Z}^2$ combinatorics where all four spheres corresponding to the vertices of a combinatorial face intersect in two real points $\mathbf{f}^+, \mathbf{f}^-$ (if the spheres intersect at all in real points).

2.3.2 Discrete Ribaucour sphere congruence. A Q-congruence of spheres is a *discrete Ribaucour congruence* if the two enveloping meshes $\mathbf{f}^+$ and $\mathbf{f}^-$ are circular meshes, i.e., if each quadrilateral face of $\mathbf{f}^+$ as well as of $\mathbf{f}^-$ has a circumcircle. Circular meshes with $\mathbb{Z}^2$ combinatorics are discrete curvature line parametrizations. The two meshes $\mathbf{f}^+$ and $\mathbf{f}^-$ are then two layers of a discrete orthogonal coordinate system [Bobenko and Huhnen-Venedey 2012].

2.3.3 Discrete central spheres. The choice of a sensible notion for a *discrete* central sphere heavily depends on the setting we are working in. We will present a Möbius invariant notion of a discrete central sphere congruence in Section 6.1 with its relevance for applications.

3 ALGORITHM

Our final goal will be fitting spheres to the faces of a mesh $M = (V, E, F)$, such that the resulting appearance is as smooth as possible. To reach that goal we will apply an optimization strategy minimizing the energy

$$E = \lambda^2_{\text{sphere}} E_{\text{sphere}} + \lambda^2_{\text{unit}} E_{\text{unit}} + \lambda^2_{\text{angle}} E_{\text{angle}}(\alpha) + \lambda^2_{\text{reg}} E_{\text{reg}} + \lambda^2_{\text{supp}} E_{\text{supp}} + \lambda^2_{\text{dual}} E_{\text{dual}} \quad (6)$$

by using the Levenberg-Marquardt algorithm [Marquardt 1963]. Variables of the optimization are the five sphere coefficients per face and the coefficients of the dual normals when $\lambda_{\text{supp}} \neq 0$. The choice of parameters and the performance of our algorithms is summarized in Table 1 for a representative set of examples.

Table 1. Default values in Eqn. (6) are defined as $\lambda_{\text{sphere}} = 1.0$, $\lambda_{\text{unit}} = 10.0$, $\lambda_{\text{angle}} = 0.1$, $\lambda_{\text{reg}} = 3.5$, $\lambda_{\text{supp}} = 1.0$, and $\lambda_{\text{dual}} = 10.0$. Times were measured using a pure Python implementation of our algorithm on a laptop with Intel i7-7500U CPU. The table exemplary lists a choice of meshes. The other meshes from Figures 9, 10, 12, 13, 14, 21, 24 behave entirely similar to the representative set of examples above.

Fig.	$\lvert F\rvert$	#iter	time/iter [sec]	residual
1	4982	40	9.8	$5.8 \cdot 10^{-2}$
3	6144	40	4.3	$7.7 \cdot 10^{-3}$
23	1766	60	0.9	$6.0 \cdot 10^{-4}$
20	2240	60	1.4	$3.3 \cdot 10^{-2}$
26	264	60	0.15	$3.3 \cdot 10^{-2}$
28	390	120	0.7	$1.1 \cdot 10^{-1}$

We will define our energy-summands in (6) throughout the paper where they appear and use matrix notations (also for inner products) for that. In general for dealing with the face spheres $f \in F$ we describe them by coefficients A, B, C, see Equation (1). All vertices $\mathbf{v} \in f$ have to satisfy the condition

$$A\mathbf{v}^2 - B^T\mathbf{v} + C = 0. \quad (7)$$

Center $\mathbf{c}$ and radius r of the corresponding sphere are determined as described after Eqn. (1). If the vertices of f are circular, there is a one-parameter family of spheres whose coefficients satisfy (7). This is always the case for $|f| = 3$ and for a circular mesh M.

The coefficients A, B, C can be initialized in three different ways: (i) using the Hessian normal form $\mathbf{n}^T\mathbf{x} = d$ of the face plane of f, (ii) as least squares sphere using the vertices of f and the vertices

of the faces adjacent to f (i.e., those faces that share an edge with f), or (iii) as central spheres in the case of a circular mesh. Without loss of generality we assume a normalization to $B^T B - 4AC = 1$.

Sphericity of mesh faces. We summarize the above conditions with the following functions defined on the faces and vertices of M

$$\varphi_{\text{sphere}}(f) = \begin{pmatrix} \mathbf{v}_{i_1}^2 & -\mathbf{v}_{i_1}^T & 1 \\ & \vdots & \\ \mathbf{v}_{i_k}^2 & -\mathbf{v}_{i_k}^T & 1 \end{pmatrix} \begin{pmatrix} A_f \\ B_f \\ C_f \end{pmatrix},$$

where $f = (\mathbf{v}_{i_1}, \ldots, \mathbf{v}_{i_k})$ and

$$\varphi_{\text{unit}}(f) = B_f^T B_f - 4A_f C_f - 1.$$

This yields derived least-squares energy terms

$$E_{\text{sphere}} = \sum\nolimits_{f \in F} \varphi_{\text{sphere}}^2(f) \quad \text{and} \quad E_{\text{unit}} = \sum\nolimits_{f \in F} \varphi_{\text{unit}}^2(f). \tag{8}$$

4 PANELING WITH SPHERICAL FACES

An advantage of using spherical faces instead of planar faces is that neither the edges nor the vertices of a face must lie in a plane, but rather on a sphere, which allows for more flexibility and smoother panel transitions. In particular, in positively curved areas of a surface the visual appeal of such panelings yields a smoother and softer appearance (see Figures 1, 3, 23, 12, 13, 20, 21, 24, and 28). The gain in flexibility is substantial as with spherical panels we do not lose planar ones since planes are spheres with infinite radius. Paneling architectural freeform skins becomes immediately more tangible if we restrict to more specific panel types [Eigensatz et al. 2010]. The isometry group of the sphere is bigger than for any other doubly curved surface, resulting in different manufacturing possibilities.

4.1 Paneling with geometric support structure

The edges of our meshes are circular arcs and therefore contained in planes. A natural and stable way to fabricate a support for such a circular arc is by materializing a segment of an annulus whose boundary curve is that circular arc (Figure 7 left). However, around a vertex all these planes carrying the circular arcs of a general sphere congruence, usually do not share a common edge but rather introduce some torsion in the node. To get torsion free nodes (see Figure 7 right) the planes carrying the circular arcs must meet in an axis – the *node axis*.

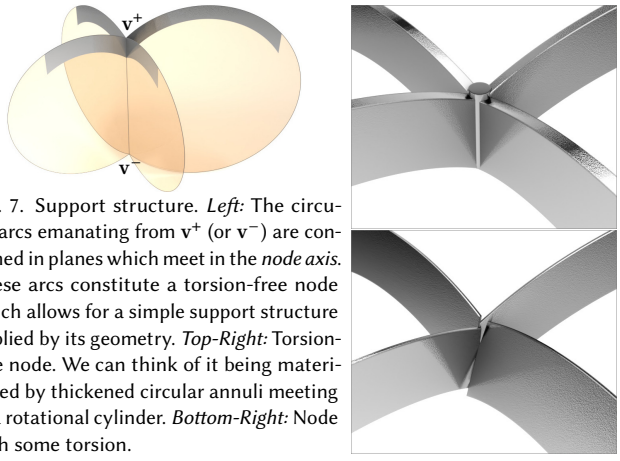

Fig. 7. Support structure. *Left:* The circular arcs emanating from $\mathbf{v}^+$ (or $\mathbf{v}^-$) are contained in planes which meet in the *node axis*. These arcs constitute a torsion-free node which allows for a simple support structure implied by its geometry. *Top-Right:* Torsion-free node. We can think of it being materialized by thickened circular annuli meeting in a rotational cylinder. *Bottom-Right:* Node with some torsion.

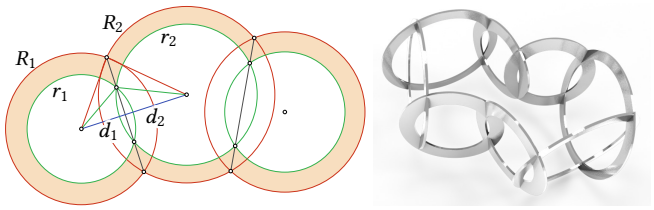

Fig. 8. *Left:* A chain of intersecting annuli. If two annuli intersect along an axis, then the outer and inner radii satisfy $R_1^2 - r_1^2 = R_2^2 - r_2^2$, which is constant along a chain of such twice intersecting annuli. *Right:* A closed chain of annuli with twice intersecting outer and inner circles.

Definition 4.1. *A* torsion free *node can be seen as a manufactured vertex star where the symmetry planes of the incoming beams intersect in a straight line (node axis). The node has some* torsion *if these planes do not intersect in an axis.*

Proposition 4.2. *A sphere mesh admits a support structure with torsion free nodes if and only if the combinatorial dual mesh consisting of the centers of the spheres has planar faces, i.e., the sphere centers around each vertex lie in a plane (Figure 7 left).*

Proof. If the centers corresponding to the spheres around a vertex $\mathbf{v}^+$ lie in a plane, then all these spheres are symmetric with respect to this plane. Consequently, they all pass through the point $\mathbf{v}^-$ which is mirror symmetric to $\mathbf{v}^+$. The line connecting $\mathbf{v}^+$ and $\mathbf{v}^-$ is the node axis of a torsion free node.

On the other hand if there exists a node axis then all planes carrying intersection circles of neighboring spheres pass through that axis. Normal to these planes are lines connecting centers of neighboring spheres. These lines must all be orthogonal to the node axis. Therefore the entire polygon of sphere centers around a vertex must lie in a plane. □

Proposition 4.3. *Sphere meshes admit a support structure with torsion free nodes if and only if the combinatorial dual mesh in the point model of Möbius geometry P^4 has planar faces.*

Proof. Proposition 4.2 and its proof imply that a sphere mesh has a support structure if and only if the spheres around each vertex intersect in two vertices $\mathbf{v}^+$ and $\mathbf{v}^-$ symmetric to the plane containing the centers. A sphere s passes through the point $\mathbf{v}^+$ if and only if $\langle\langle \hat{\mathbf{v}}^+, \hat{\mathbf{p}} \rangle\rangle = 0$ (cf. Equation (3)). Likewise $\langle\langle \hat{\mathbf{v}}^-, \hat{\mathbf{p}} \rangle\rangle = 0$. Hence, all spheres through $\mathbf{v}^+$ and $\mathbf{v}^-$ are represented in P^4 as a two-dimensional plane defined by $\langle\langle \hat{\mathbf{v}}^+, \hat{\mathbf{p}} \rangle\rangle = \langle\langle \hat{\mathbf{v}}^-, \hat{\mathbf{p}} \rangle\rangle = 0$. □

The proof of Proposition 4.3 suggests that all spheres represented by the points of a two-dimensional plane τ in P^4 meet in two points. These two intersection points coincide if τ is tangent to the sphere S^3: $\langle\langle \mathbf{x}, \mathbf{x} \rangle\rangle = 0$, or are imaginary if τ intersects S^3 in a real circle.

The annuli forming the support structure of a spherical face can be arranged to bridge concentric spheres as outer and inner layer. Each of the two boundary circles of each annulus intersects the corresponding boundary circle of an adjacent annulus in two points, i.e., the annuli have twice intersecting boundary circles. This

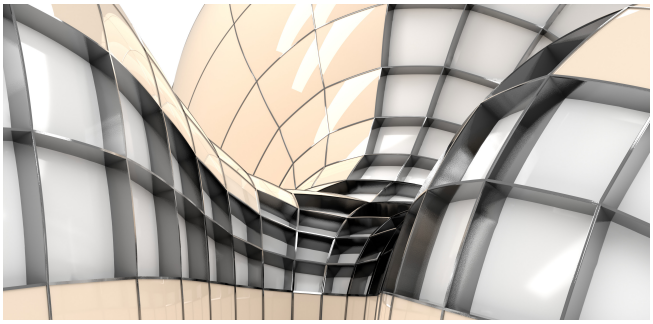

Fig. 9. Surface from Figure 28 optimized for the existence of a geometric support structure. The planes carring the circular edge-arcs around a vertex meet in an axis. Proposition 4.2 implies that the dual mesh of the centers of the spheres necessarily form a mesh with planar faces which is shown in Figure 28 (bottom-right). To see inside we removed some panels of the outer layer. This support structure consists of (parts of) chains of twice intersecting annuli as depicted in Figure 8.

propagates through the entire mesh (see Lemma 4.4 and Figure 8 for such chains and Figure 9 for an image on how it could be applied).

Lemma 4.4. *Any closed chain of twice intersecting circles comes with a one-parameter family of interconnected annuli (see Fig. 8 right).*

Proof. If the boundary circles of two annuli intersect each other twice we have the relation (see Figure 8 left)

$$R_1^2 - d_1^2 = R_2^2 - d_2^2 \quad \text{and} \quad r_1^2 - d_1^2 = r_2^2 - d_2^2,$$

where R_i denotes the radius of the outer circle, r_i the radius of the inner circle, and d_i the distance of the center to the node axis. Therefore, $R_1^2 - r_1^2 = R_2^2 - r_2^2$ which is a constant along a sequence of twice intersecting annuli: $R_i^2 - r_i^2 = \text{const}$. Consequently, any (closed) chain of twice intersecting circles with radii R_i can be extruded to twice intersecting annuli with second boundary circle radius r_i such that $R_i^2 - r_i^2 = \text{const}$. There is one degree of freedom, e.g., the choice of r_1, but not all choices of r_1 might lead to real intersections. □

We enforce the existence of such a geometric support structure by adding a planarity term E_{supp} to the faces of the mesh of sphere centers in our optimization (Sec. 3). Planarity of the faces of the mesh of centers yields the theoretical existence of the geometric support structure. However, the planes carrying the circular annuli can lie rather tangential to the surface resulting in practically undesirable situations. We therefore add a regularization term E_{reg} to our optimization which enforces these planes to be as close as possible to the bisector planes of the corresponding faces. See Figure 9 for a paneling with support structure.

Regularization energy. The plane carrying the circle we get from intersecting two spheres $(\mathbf{c}, r)$ and $(\mathbf{c}', r')$ is orthogonal to the direction $\mathbf{c} - \mathbf{c}'$. We want this plane to be close to the bisector plane of neighboring faces f and f'. Let $\mathbf{n}$ and $\mathbf{n}'$ be the face normals of f and f', respectively. The vector $\mathbf{n}_e = \mathbf{n} + \mathbf{n}'$ can be seen as a discrete edge normal vector. Hence $\mathbf{c} - \mathbf{c}'$ has to be orthogonal to the direction vector of the edge $e = (\mathbf{u}, \mathbf{w})$ and the vector $\mathbf{n}_e$. Expressing sphere centers in terms of corresponding coefficients of Equation (1), this condition can be written as

$$\varphi_{\text{reg}}(e) = \begin{pmatrix} \mathbf{n}_e^T \\ (\mathbf{u} - \mathbf{w})^T \end{pmatrix} (A_f B_{f'} - A_{f'} B_f) = 0.$$

The derived energy reads

$$E_{\text{reg}} = \sum\nolimits_{e \in E} \varphi_{\text{reg}}^2(e).$$

Energy for the existence of geometric support structure. Vanishing of the regularization energy does not imply the existence of a geometric support structure, i.e., the planes obtained by pairwise intersection of spheres around a vertex might not intersect in a line (except for so called conical meshes where the bisector planes around a vertex $\mathbf{v}$ always meet in a line that coincides with the cone axis (discrete normal) of vertex $\mathbf{v}$; see [Liu et al. 2006]).

This is only true if the dual face formed by the centers of involved spheres is planar (cf. Prop. 4.2); the node axis of a geometric support structure is a normal of the dual face.

Let $\mathbf{n}_*$ be a least squares estimate of the dual normal, i.e., the normal of the dual face and $(f_{i_1}, \ldots, f_{i_k})$ the incident faces of a vertex $\mathbf{v} \in V$. The centers of the assigned face spheres are the vertices of the dual face. For notational convenience the sphere coefficients associated with f_{i_j} are denoted by A_j, B_j, C_j. We define

$$\varphi_{\text{supp}}(\mathbf{v}) = \begin{pmatrix} (A_1 B_2 - A_2 B_1)^T \\ (A_2 B_3 - A_3 B_2)^T \\ \vdots \\ (A_k B_1 - A_1 B_k)^T \end{pmatrix} \mathbf{n}_* \quad \text{and} \quad \varphi_{\text{dual}}(\mathbf{v}) = \mathbf{n}_*^T \mathbf{n}_* - 1.$$

The associated energies are

$$E_{\text{supp}} = \sum\nolimits_{\mathbf{v} \in \mathring{V}} \varphi_{\text{supp}}^2(\mathbf{v}) \quad \text{and} \quad E_{\text{dual}} = \sum\nolimits_{\mathbf{v} \in \mathring{V}} \varphi_{\text{dual}}^2(\mathbf{v}),$$

where $\mathring{V}$ denotes the non-boundary vertices of the mesh M.

4.2 Angle minimizing panels

One of the aims of our paper is paneling surfaces in such a way that the generated surface skin is smoother than with planar faces. A mesh with spherical panels is the smoother the smaller the intersection angle between neighboring sphere tiles is. We propose an energy that minimizes the sum of intersection angles and can easily be adapted to optimize for any other prescribed intersection angle (see Sec. 3 for the energy and Figure 10 for an SQ-mesh constant intersection angle of $\pi/3$).

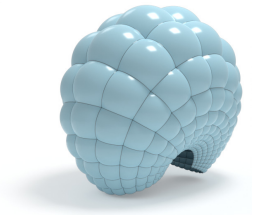

Fig. 10. Minimization of intersection angles is not the only goal that can be achieved with the energy term E_{angle}, see Eqn. (9). It can easily be adapted to optimize for any prescribed angle resulting in interesting surface features. The image depicts an SQ-mesh optimized for intersection angles as close as possible to $\pi/3$.

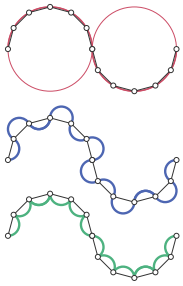

Let us explain some *difficulties and counterintuitive phenomena* that can arise. Consider (for simplicity) a polygon with three different corresponding circular edges (see *inset*). The two upper examples are angle-minimizing realizations as neighboring circles perfectly touch each other. However the difficulty arises on where they should touch, from the outside or inside. The preferred smoother solution is the upper one where all 12 arcs coincide with only two touching circles. The example in the middle is C^1 continous but rather "bumpy". The bottom solution, where all 12 circles have the same radius and where neighboring circles have the same tangent, is *not* C^1 continuous. This "spiky" example provides a visually nice feature but produces a non-smooth surface effect (see also Fig. 27 left).

Initialization. The central sphere congruence (Sec. 2.2.5) consists of spheres whose radii are the harmonic mean of the principal curvature radii. Consequently, central spheres represent an average of the local curvature. A sensible discretization of the central spheres (see Sec. 6.1 for SQ-meshes) therefore constitutes a good initialization for our angle minimizing algorithm.

Another simple idea for finding face spheres in a circular mesh with an expectable low angle sum is the following. We insert vertices per face (Figure 11 center) which together with the circumcircle of the face determine the face sphere. We consider the triangle mesh consisting of these newly inserted vertices per face together with the vertices of the original circular mesh. Then we apply Laplacian smoothing to this triangle mesh while keeping the original vertices fixed. The so obtained spheres (Figure 11 right) can be used as initialization for our angle minimizing algorithm or – as we experienced in practice – constitute already a good result. Note that spheres resulting from Laplacian smoothing are not Möbius invariantly connected to the circular mesh, but provide in practical applications already good solutions.

Even more flexible than that is the initialization of our optimization with best fitting spheres through the vertices of the face and its 1-ring neighbors. For that we solve a least squares system for A, B, C from Eqn. (1). The advantage of this method is that the given mesh does not have to be perfectly circular and the spherical faces do not have to absolutely pass through the given vertices of the mesh. We can easily make use of manufacturing tolerances which are always present in applications. In this way we obtain solutions

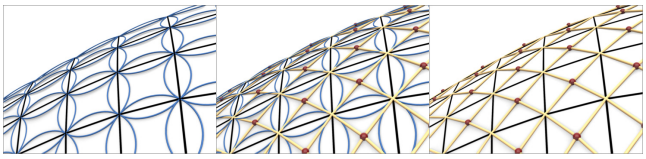

Fig. 11. Sphere meshes from Laplacian smoothing. *Left:* A given circular mesh. *Center:* We insert vertices per face and connect them with the original vertices to a triangle mesh. *Right:* Laplacian smoothing while keeping the original vertices fixed results in a fair triangle mesh. The inserted vertices together with their circular 1-rings determine a sphere per each face.

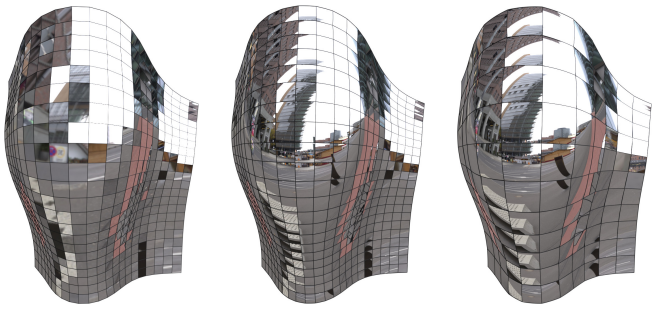

Fig. 12. Comparison of two different levels of discretization of sphere meshes to the mesh with planar faces. The original circular mesh (*left*) has a rougher appearance than the SQ-meshes; with equal number of faces (*center*) and with only a quarter as many faces (*right*). The visual smoothness between the two SQ-meshes is comparable.

where we can treat the vertices of the mesh as variables which are then also subject to optimization, yielding more flexible solutions within tolerances.

Multiple scales. The usage of spherical faces instead of planar faces can contribute to a reduction in the number of panels while still increasing its smoothness. In Fig. 12 we compare different scales of "facattedness" and their visual smoothness by looking at reflections.

Smoothness energy. If f and f' are two neighboring faces with common edge e, the transition between corresponding spheres across e is smooth or angle minimizing when

$$B_f^T B_{f'} - 2(A_{f'} C_f + A_f C_{f'})$$

is close to ± 1, see Equation (5). Note that this assumes that the used sphere coefficients are normalized. A non-smooth appearance can be generated by replacing 1 with $\cos(\alpha)$ where $\alpha \in [0, \pi/2]$ is the target intersection angle of neighboring spheres, see Figure 10 for an example. We get

$$\varphi_{\text{angle}}(e, \alpha) = \left(B_f^T B_{f'} - 2(A_{f'} C_f + A_f C_{f'})\right)^2 - \cos^2(\alpha)$$

and derived energy

$$E_{\text{angle}}(\alpha) = \sum\nolimits_{e \in E} \varphi^2_{\text{angle}}(e, \alpha). \tag{9}$$

4.3 Radii clustering

To simplify the manufacturing process it might be important to reduce the variety of different sphere radii to a manageable amount. The big sphere of the *Nur Alem Museum of Future Energy* (Figure 2) consists clearly of sphere patches with just one radius. Our experiments show that even on more complicated shapes, i.e., meshes which exhibit a much wider curvature variation, a rather small number of radii provides already a very good solution in the sense of visual smoothness (see Figures 13 and 14). For that we use the k-means method to partition our spheres into k clusters. After fixing the sphere radii we run an optimization step to let the mesh relax with the newly chosen spheres. Depending on applications, materials, scale and budget the designer/user can choose how many different sphere radii should be used.

5 TRIANGULAR SPHERE MESHES

The existence of a support structure for a sphere mesh is characterized by Prop. 4.2 and 4.3. However, it turns out that the combinatorics of a sphere mesh implies special properties and interesting construction methods. We therefore distinguish between sphere meshes with hexagonal (Sec. 7), quadrilateral (Sec. 6), and triangular combinatorics (Sec. 5). We start in this section with the latter.

We will see that face spheres of triangular sphere meshes with support structure are orthogonal to a real or imaginary sphere, or pass through a point. They can therefore be interpreted as polyhedral meshes in conformal models of classical non-Euclidean geometries.

The results of the following sections should be usable even for readers without any knowledge of non-Euclidean geometry.

Proposition 4.3 implies that an STriangle-mesh admits a support structure if the combinatorial dual mesh consisting of the representatives of the face spheres $\hat{\mathbf{s}}$ in P^4 form a trivalent mesh with planar faces (generically a *PHex-mesh*, i.e., a hexagonal mesh with planar faces). Except stated otherwise we will therefore until the end of this section only consider trivalent meshes $\hat{\mathbf{s}} \in P^4$ with planar faces. Two neighboring planar faces in a trivalent vertex star of $\hat{\mathbf{s}}$ in P^4 intersect along a common edge and therefore span at most a three-dimensional subspace Γ of P^4. The third face in the vertex star is spanned by two edges already contained in Γ and is therefore also contained in Γ. Propagating this reasoning, the entire mesh $\hat{\mathbf{s}}$ is contained in Γ. Consequently, we have:

Lemma 5.1. *The P^4-representatives $\hat{\mathbf{s}}$ of the face spheres of an STriangle-meshes with support structure form a trivalent polyhedral mesh contained in a three-dimensional subspace $\Gamma \subset P^4$.*

The pole $\hat{\omega} \in P^3$ of the three-dimensional hyperplane Γ with respect to S^3 is a point representing a sphere ω that is orthogonal to all spheres represented by the points in Γ (cf. end of Sec. 2.1). This sphere ω can be real, imaginary or degenerate to a point. A real sphere intersects an imaginary sphere $\|\mathbf{x}-\mathbf{c}\|^2 = -r^2$ orthogonally if it intersects its so-called *real representative* $\|\mathbf{x}-\mathbf{c}\|^2 = r^2$ along a great circle. We summerize the above in the following proposition.

Proposition 5.2. *The face spheres of an STriangle-mesh with support structure come in three types depending on ω:*

(i) ω is a real sphere and all face spheres are orthogonal to ω.

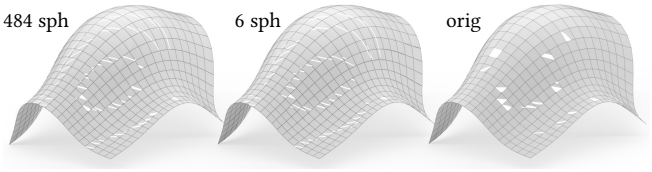

Fig. 13. Radii clustering. Given a circular mesh with 484 faces (*right*). We compute angle minimizing SQ-meshes and cluster by radii. The light reflections come from light sources in form of three parallel straight lines. *Left:* No clustering; spheres with 484 different radii. *Center:* Spheres with 6 different radii. Note that the differences in smoothness of the reflection curves between the SQ-meshes is rather small, but the difference to the original mesh with planar faces (*right*) is notable. Even the SQ-mesh with only 6 different spheres has a much smoother appearance. The clustering of the 6 spheres is depicted in Figure 14.

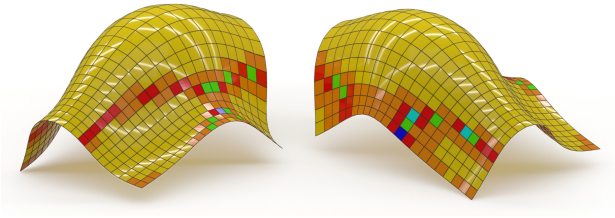

Fig. 14. Two views of the mesh from Figure 13 as SQ-mesh with sphere patches taken from just 6 different spheres. The faces filled out with the same sphere have the same color. The radii clustering has been done with the k-means method (see Sec. 4.3).

(ii) ω is an imaginary sphere and all face spheres intersect a fixed sphere (the real representative *of ω) in a great circle.*

(iii) ω is a point and all face spheres pass through this point ω.

In all three cases, the planes and node axes of the support structure pass through the center of ω.

The classification in types (i) to (iii) follows from the above and the node axes property follows from the discussion below.

These three types have nice interpretations in terms of non-Euclidean geometries. Non-Euclidean geometries are often studied in several models such as the projective or the conformal model (see, e.g., [Klein 1968]). We exploit the transition between the aforementioned models. Knowledge of non-Euclidean geometry is not needed to utilize the results of the following sections. Just apply the maps from equations (10) and (11) according to Propositions 5.3 and 5.6, respectively. The following three sections discuss the three different cases of Proposition 5.2.

5.1 Hyperbolic meshes

In the case of Proposition 5.2 (i), the face spheres can be interpreted as planes in the *Poincaré* model of hyperbolic 3-space. Planes in this model appear as spheres which intersect the boundary sphere orthogonally. Consequently, we see spherical faces with our Euclidean

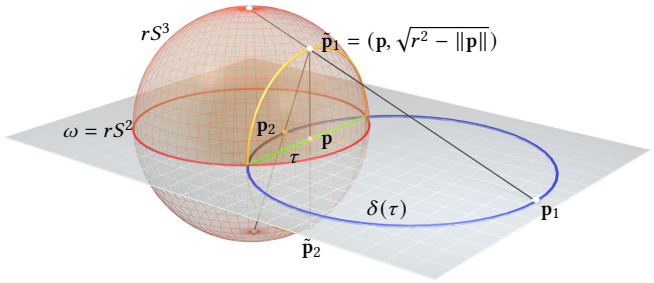

Fig. 15. Model change from the Cayley-Klein model of hyperbolic geometry inside the absolute sphere rS^2 to the Poincaré model including ideal points. A point $\mathbf{p}$ is mapped to two points $\delta(\mathbf{p}) = \mathbf{p}_{1,2}$ first via vertical projection onto the sphere rS^3 and then stereographically projected into the hyperplane. This sequence of transformations maps a plane τ first onto a sphere on rS^3 and then to a sphere in the hyperplane. Note that this image is an illustration of a four-dimensional setting. We therefore illustrate, for example, the two-dimensional sphere rS^2 as circle.

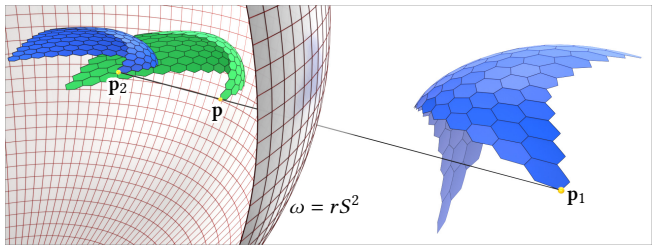

Fig. 16. Model change from the Cayley-Klein model inside the absolute sphere $\omega = rS^2$ to the Poincaré model including ideal points. The green PHex-mesh with vertex $\mathbf{p}$ is given inside rS^2. Applying δ yields two SHex-meshes with support structure with vertices $\mathbf{p}_1$ outside and $\mathbf{p}_2$ inside ω. The two points $\mathbf{p}_1$ and $\mathbf{p}_2$ are related by a Möbius inversion in the sphere ω.

eye, but within hyperbolic geometry the faces are actually flat. In the *Cayley-Klein* model of hyperbolic geometry the hyperbolic planes appear as planes in real projective space. We use $\omega = rS^2$ as absolute sphere defining the hyperbolic metric. The transition between the two models is depicted in Fig. 15. For that, the Cayley-Klein model, is embedded as a hyperplane in a four-dimensional space by adding an x_4-coordinate. The absolute sphere is now the "equator" of the three-dimensional sphere rS^3. A point $\mathbf{p}$ on the inside of the absolute sphere in the Cayley-Klein model is orthogonally projected in x_4-direction to two points $\tilde{\mathbf{p}}_1, \tilde{\mathbf{p}}_2$ of the sphere rS^3. These points are then stereographically projected back to the equator plane to obtain $\mathbf{p}_1, \mathbf{p}_2$. This double-valued function δ transforms points $\mathbf{p}$ from the Cayley-Klein model to point pairs $\mathbf{p}_1, \mathbf{p}_2$ in the Poincaré model. It is easily determined with the help of Fig. 15 and reads

$$\delta(\mathbf{p}) := \mathbf{p}_{1,2} = \|\mathbf{p}\|^{-2}\big(r^2 \pm r\sqrt{r^2 - \|\mathbf{p}\|^2}\big)\mathbf{p}. \tag{10}$$

The map δ transforms planes inside ω to spheres orthogonally intersecting the sphere ω. We can easily convince ourselves of this fact in one dimension lower (as depicted in Fig. 15): The vertical projections of lines to the sphere are circles intersecting the equator orthogonally, a property which is kept by the stereographic projection.

This model change yields a very simple description as well as construction method for all STriangle-meshes of type 5.2 (i):

Proposition 5.3. *STriangle-meshes with support structure of type 5.2 (i) are the images of triangle meshes with planar faces contained in a sphere $\omega = rS^2$ under the transformation δ from Equation* (10). *See Figure 17 for examples.*

Remark 5.4. Note that the position of the triangle mesh with respect to the absolute sphere ω has an influence on the result. Furthermore note that $\langle \mathbf{p}_1, \mathbf{p}_2 \rangle = r^2$. This implies that $\mathbf{p}_2$ is a reflection (Möbius inversion) of $\mathbf{p}_1$ in the sphere ω (see Fig. 16). This confirms the node-axis property from Prop. 5.2. Thus, the two STriangle-meshes resulting from δ only differ by a Möbius transformation.

Remark 5.5. Clearly, any other mesh with planar faces that is contained in the Cayley-Klein model of hyperbolic geometry can be transformed into a sphere mesh via model change δ. See Figure 17 (bottom-row) for an SHex-mesh constructed this way. Note that in the hexagonal or quadrilateral case this method only produces a subclass of sphere meshes with support structure.

5.2 Elliptic meshes

In the case of Proposition 5.2 (ii), the face spheres can be interpreted as planes in the *conformal* model of elliptic 3-space. Planes in this model appear as spheres which intersect the real representative of ω in a great circle. We see spherical faces with our Euclidean eye, but within elliptic geometry the faces are flat. In the *Cayley-Klein* model of elliptic geometry, the elliptic planes appear as planes in real projective space (with a distinguished imaginary sphere as absolute sphere defining the elliptic metric). The transition between the two models is depicted in Figure 18 and works in complete analogy to the hyperbolic case (Sec. 5.1). We therefore only give the formula

$$\delta(\mathbf{p}) := \mathbf{p}_{1,2} = \|\mathbf{p}\|^{-2}\big(-r^2 \pm r\sqrt{r^2 + \|\mathbf{p}\|^2}\big)\mathbf{p}. \tag{11}$$

Proposition 5.6. *STriangle-meshes with support structure of type 5.2 (ii) are the images of arbitrary triangle meshes with planar faces under the transformation δ from Eqn.* (11). *See Fig. 19 for examples.*

5.3 Sphere bundle meshes

In case 5.2 (iii), the face spheres pass through a fixed point. A Möbius transformation mapping this point to infinity maps all face spheres to Euclidean planes and the STriangle-mesh to a polyhedral surface.

Proposition 5.7. *STriangle-meshes with support structure of type 5.2 (iii) are Möbius transforms of triangular meshes with planar faces.*

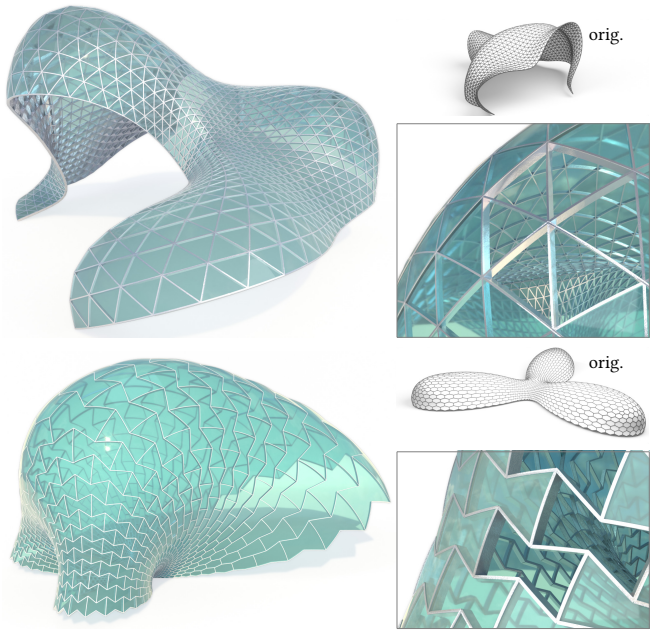

Fig. 17. STriangle-mesh with detail and original (*top-row*) and SHex-mesh with detail and original (*bottom-row*) resulting from a model change of hyperbolic geometry. The existence of the support structure follows automatically from its generation (cf. Proposition 5.3 and Sec. 5.1).

5.4 STriangle meshes without support structure

For any *triangle mesh* we can replace its planar faces by spherical faces passing through the three vertices of the face. The spheres are therefore members of the elliptic sphere pencil determined by the circumcircle of the triangular face. An optimization with a good choice of initial spheres (like fitting the sphere to the triangle plus its 1-ring) converges very quickly to an optimal angle minimizing solution (see Figure 20). Even surfaces minimizing a discrete Willmore energy (under some constraints; see, e.g., [Soliman et al. 2021]) which are by itself already as-spherical-as-possible polyhedral triangular meshes benefit from paneling with angle minimizing spherical faces as illustrated by Figure 21.

6 QUADRILATERAL SPHERE MESHES

In contrast to sphere meshes with triangular combinatorics (Sec. 5), in the quadrilateral case the existence of a support structure does not imply that the sphere mesh is a polyhedral mesh in a non-Euclidean geometry. The face spheres of a general polygonal quad mesh are uniquely determined by the four vertices of the faces. In the case of circular meshes though there is a one-parameter family of spheres per face to choose from. Within this family, the so called central spheres known in Möbius geometry are very close to angle minimizing spheres.

6.1 Discrete central spheres

The classical central sphere (see Sec. 2.2) is a particular sphere of the parabolic sphere pencil touching the smooth surface in a surface point. Such a parabolic sphere pencil contains a distinguished Möbius invariant sphere, namely the point sphere $\mathbf{f}$, which is used to define the central sphere as that sphere s_z for which $\mathrm{cr}(\hat{\mathbf{s}}, \hat{\mathbf{f}}, \hat{\mathbf{s}}', \hat{\mathbf{s}}_z) = -1$ holds, where s and s' are the principal curvature spheres. Therefore the central sphere is also Möbius invariant. Note

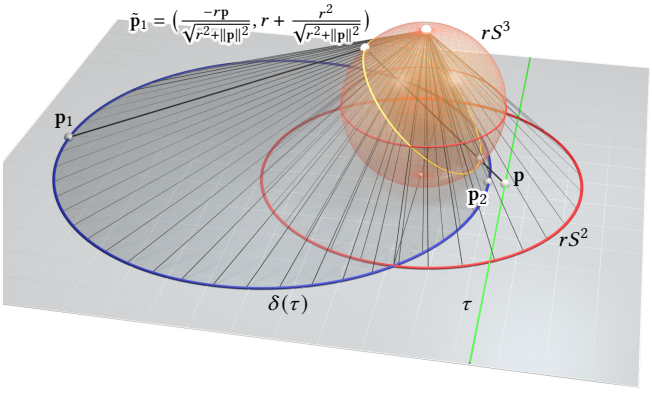

Fig. 18. Model change from the Cayley-Klein model of elliptic geometry in the projective space with an imaginary absolute sphere represented by its real representative rS^2 to the conformal model. A point $\mathbf{p}$ is mapped to two points $\delta(\mathbf{p}) = \mathbf{p}_{1,2}$ first via central projection onto the sphere rS^3 and then stereographically projected into the hyperplane. This sequence of transformations maps a plane τ first onto a sphere on rS^3 and then to a sphere in the hyperplane. Note that this image is an illustration of a four-dimensional setting. We therefore illustrate, for example, the two-dimensional sphere rS^2 as circle.

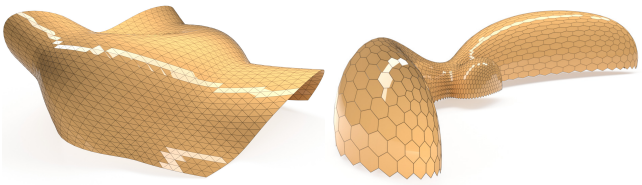

Fig. 19. STriangle-mesh (*left*) and SHex-mesh (*right*) resulting from a model change of elliptic geometry. The existence of the support structure follows automatically from its generation (cf. Proposition 5.6 and Sec. 5.2).

that in an elliptic sphere pencil there is no distinguished Möbius invariant sphere. However, for paneling circular meshes with spherical faces, which come naturally with an elliptic sphere pencil per face, it would be beneficial to have a central sphere that we could use to initiate our algorithm.

Circular meshes with $\mathbb{Z}^2$ combinatorics have two-parameter families of edge-parallel Gauss images [Bobenko et al. 2010]. Any such Gauss image gives rise to a vertex-based congruence of parabolic sphere pencils forming a so called contact element net [Bobenko and Suris 2008]. However, with the view towards panelization, it is more useful to consider spheres per face instead of vertices.

Let us consider a face f with its four neighboring faces f_i, f_j, f_k, f_l (see Figure 22 left). Two circumcircles of two edge-adjacent faces, say of f and f_i, intersect in two points and therefore span a unique sphere s_i. This sphere estimates the principal curvature in the direction transversal to the common edge and belongs to the elliptic sphere pencil of the circumcircle of f. So we obtain a sphere per edge. Consequently two opposite edges in a face give rise to two spheres s_i and s_k. They belong to an elliptic sphere pencil. We can therefore define the angle bisecting sphere of s_i and s_k (bisecting the

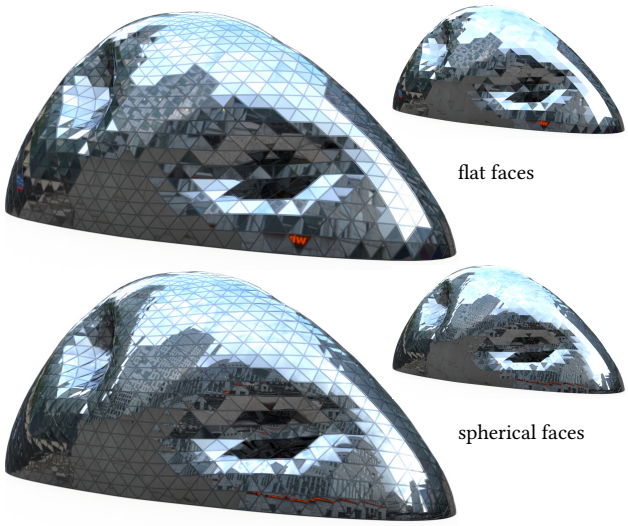

Fig. 20. *Top:* A triangle mesh (*The Blob* by M. Fuksas) with *flat* faces – with (*left*) and without edge beams (*right*). *Bottom:* An angle minimizing STriangle mesh – with (*left*) and without edge beams (*right*). Note that the reflection of the surrounding in the STriangle mesh is much smoother.

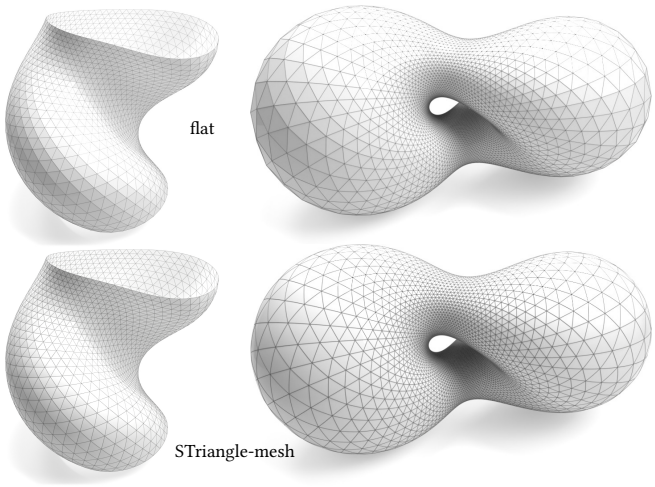

Fig. 21. Surfaces minimizing a discrete Willmore energy (*top-row* with flat faces) become locally as spherical as possible under some constraints such as the conformal class (constrained Willmore surfaces) and given boundary data as depicted in the image (cf. [Soliman et al. 2021]). It seems natural to panel such surfaces with angle minimizing spherical faces (*bottom-row*). Note that the already quite smooth surface appears even smoother with the angle minimizing spherical faces.

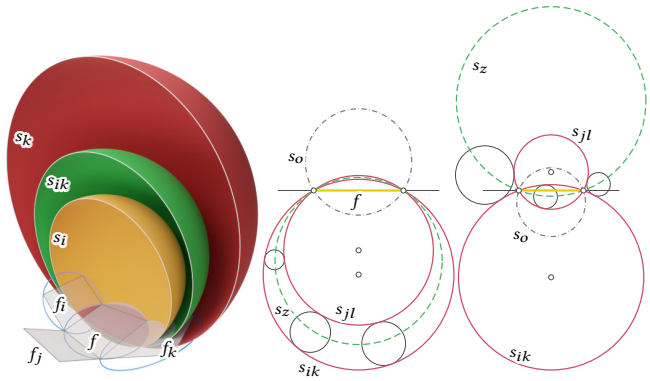

Fig. 22. Elliptic sphere pencil with central sphere. *Left:* The circumcircles of two neighboring faces f, f_i [or f, f_k] span a sphere s_i [or s_k] belonging to the elliptic sphere pencil spanned by the circumcircle of f. Both spheres s_i and s_k represent principal curvature spheres corresponding to edges. Averaging both by taking the angle bisecting sphere s_{ik} defines a principal curvature sphere for the direction ik at face f. *Center and right:* The sphere s_z bisecting the smaller angle of the two principal curvature spheres s_{ik} and s_{jl}, is the discrete central sphere. The central sphere intersects a family of s_{ik} and s_{jl} twice touching spheres orthogonally (cf. Sec. 6.1).

smaller angle) as the *principal curvature sphere* s_{ik} corresponding to the direction ik at f. By angle bisecting we mean that the normal vector of the "bisecting sphere" bisects the two normal vectors of the two given spheres at a common point of the intersection circle of the three spheres. Analogously we construct the other principal curvature sphere s_{jl}. The pentaspherical coordinates of the bisecting sphere can easily be computed using the formula presented in the following lemma which we prove in the appendix (Sec. A.2)

Lemma 6.1. *Let s_i, s_k with radii r_i, r_k be two intersecting spheres generating an elliptic sphere pencil. Their pentaspherical coordinates are denoted by $\hat{\mathbf{s}}_i, \hat{\mathbf{s}}_k$. Then the angle bisecting spheres are given by*

$$\hat{\mathbf{s}}_{ik} = \varepsilon r_k \hat{\mathbf{s}}_i + r_i \hat{\mathbf{s}}_k, \qquad \hat{\mathbf{s}}_o = \varepsilon r_k \hat{\mathbf{s}}_i - r_i \hat{\mathbf{s}}_k$$

where $\varepsilon := \operatorname{sign}\langle\langle \hat{\mathbf{s}}_i, \hat{\mathbf{s}}_k \rangle\rangle$. The acute angle is bisected by $\hat{\mathbf{s}}_{ik}$.

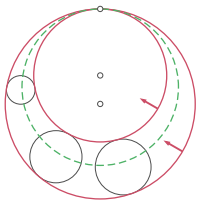

The central sphere (green dashed) in a point of a smooth surface is geometrically characterized as that sphere which is orthogonal to all spheres of a sphere congruence that touch the oriented principal spheres (red) in different orientations (cf. [Blaschke 1929, p. 299]). In analogy to this geometric characterization we characterize the discrete central sphere as that sphere which intersects all spheres of a twice touching sphere congruence orthogonally. However, two spheres of an elliptic sphere pencil do not determine such a sphere congruence uniquely but rather two (in contrast to a parabolic sphere pencil). One congruence lies between the acute angle formed by the two spheres, the other one between the obtuse angle (see Figure 22 center and right). Consequently, we define the *discrete central sphere* as that sphere which intersects the twice touching sphere congruence between the acute angle orthogonally. Equivalently, the discrete central sphere is characterized as that angle bisecting sphere which lies in the acute angle between the two discrete principal curvature spheres (see Figure 22 center and right). The discrete central sphere s_z has a simple description in its pentaspherical coordinates $\hat{\mathbf{s}}_z$ as computed in analogy to Lemma 6.1 with $\varepsilon = \operatorname{sign}\langle\langle \hat{\mathbf{s}}_{ik}, \hat{\mathbf{s}}_{jl} \rangle\rangle$:

$$\hat{\mathbf{s}}_z = \varepsilon r_{jl} \hat{\mathbf{s}}_{ik} + r_{ik} \hat{\mathbf{s}}_{jl}.$$

6.2 Angle minimizing SQ-meshes

Each planar face of a *circular quad mesh* can be replaced by a spherical face chosen from the one-parameter family of spheres through the circumcircle of the face. Our numerical optimization results (see Sec. 3) confirm our concept that the central sphere congruence (Sec. 2.3) is already very close to the numerical angle minimization result. Compare, for example, the images in Figure 26.

Circular meshes with *mixed combinatorics* like the semi regular tesselation in Fig. 3 or the hybrid mesh ("The Cour Visconti" in the Louvre) in Fig. 23 can be transformed into an intersection angle minimizing sphere mesh in the same way. However in that case we do not have a concept of discrete central spheres. The optimization algorithm was initialized with locally best fitting spheres (see Sec. 3).

6.3 Strip formation

The angle minimizing spheres which are close to the central spheres approximate surfaces very smoothly and yield a different perception of the surface than a realization with planar faces would. Since the angle minimizing face spheres are very close to the central spheres, the curvature of these face spheres approximates the arithmetic mean of the principal curvatures. An interesting visual effect appears when we use spherical patches which do not approximate the central sphere but rather the principal spheres in one direction. It generates

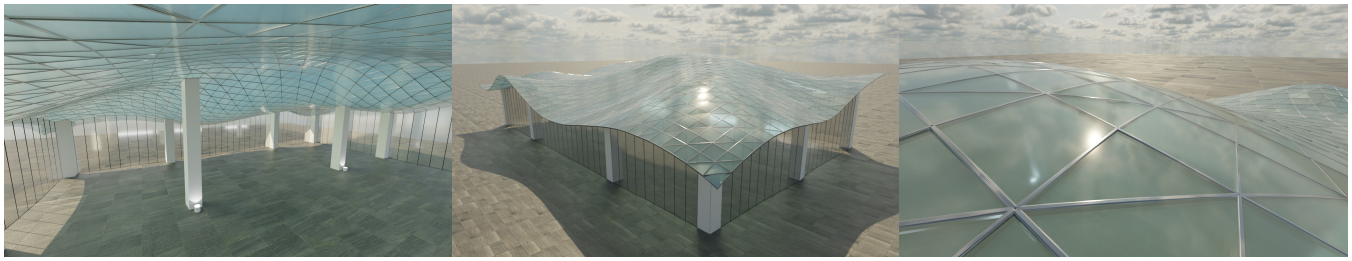

Fig. 23. A hybrid mesh of spherical quadrilaterals and spherical triangles optimized for minimal intersection angle.

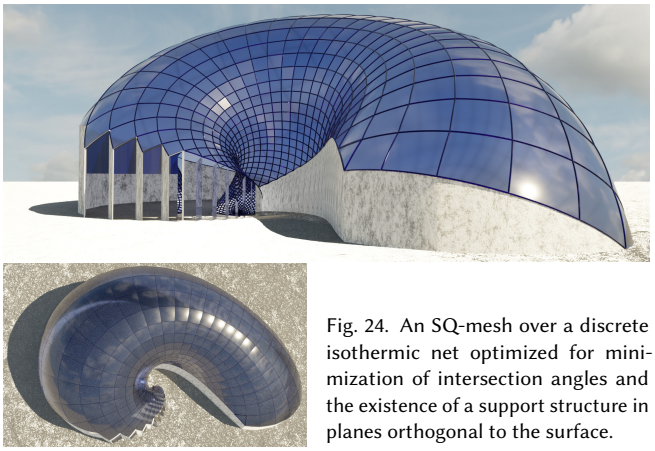

Fig. 24. An SQ-mesh over a discrete isothermic net optimized for minimization of intersection angles and the existence of a support structure in planes orthogonal to the surface.

curved strips along parameter curves of the surface (see Figures 1 and 25). This can be interpreted as approximating a surface with a discrete sequence of canal surfaces.

6.4 SQ-remeshing

Suppose we want to approximate a given surface $\mathcal{M}$ by an SQ-mesh with support structure. We could first approximate $\mathcal{M}$ with a circular mesh and apply our strategies from the previous paragraphs, but we actually have more degrees of freedom. The vertices of a spherical face of a sphere mesh do not have to lie on a circle. It follows from Proposition 4.3 that the only thing we need is a PQ-mesh in P^4 whose corresponding spheres approximate $\mathcal{M}$.

We therefore propose a *remeshing* strategy to approximate an arbitrary given sphere mesh or sphere congruence by an SQ-mesh with support structure whose faces are not necessarily circular.

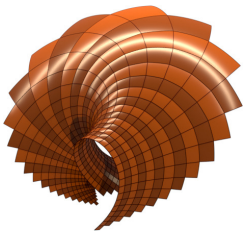

Fig. 25. Strip formation. In negatively curved surface areas angle minimizing sphere meshes tend to form strips (see also Figure 1). Since this phenomenon has been identified as design feature we intensify it by enforcing the angle minimizing term only on selected edges and neglecting or strongly reducing it on the others.

This amounts to remeshing a surface in P^4 into a PQ-mesh. The input sphere mesh that approximates $\mathcal{M}$ could be generated for example by intersecting tangential spheres as described in Sec. 7.

A comparable task is the remeshing of a triangular mesh in $\mathbb{R}^3$ into a PQ-mesh or a discrete principal mesh. While the result of remeshing by a principal mesh is to some extent intuitively guessable from its geometric shape, the result of our new remeshing scheme is less obvious.

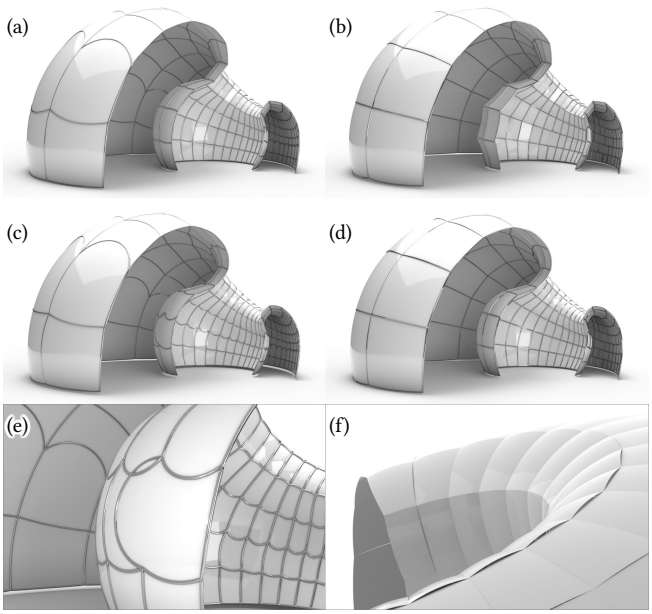

Fig. 26. A circular mesh with different types of sphere panels. (a) No optimization. The spherical panels are the discrete central spheres as described in Sec. 2.3. Edges are intersection circles of neighboring spheres. (b) Edges are intersection circles of neighboring spheres. These edges are enforced to lie in bisector planes of neighboring faces. Note that the centers of the sphere are therefore enforced to lie on one side of the surface. This can imply the feature of spiky sphere panels in positively curved regions. (c) Optimization for minimal angle but no additional constraints. Edges are intersection circles of neighboring spheres which can lie in planes very tangential to the surfaces and produce counterintuitive artifacts (e). (d) Edges are intersection circles of spheres with bisector planes of neighboring faces. The gaps that arise between two neighboring spheres are illustrated in (f).

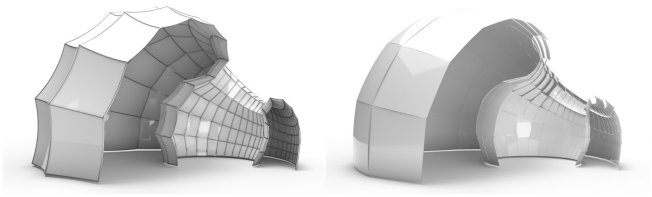

Fig. 27. Importance of initialization. The image on the *left* is obtained by reflecting the discrete central spheres in the faces. The spiky features might give an appealing appearance but are in general not close to angle minimizing anymore. The centers of this spheres in comparison with an optimal result lie in the wrong side of the surface. Our angle optimizer runs into a local minimum (*right*) which is not an optimal solution (see Figure 26).

We consider a given sphere congruence, for example, with triangle combinatorics. Thus the sphere congruence is a triangulated surface in the point model of Möbius geometry P^4. We know that the desired SQ-mesh is represented in P^4 as PQ-mesh. We therefore have to remesh the given triangle mesh in P^4 into a PQ-mesh in P^4 which is not a standard task in geometry processing. For smooth surfaces that would mean to find a *conjugate* parametrization on the given surface in P^4.

While surfaces in $\mathbb{R}^3$ have many conjugate parametrizations (we can freely choose a one-parameter family of parameter curves) in four-dimensional space $\mathbb{R}^4$ the conjugate parametrization is unique (see, e.g., [Bobenko and Suris 2008, p. 2]). Note that this conjugate parametrization is not necessarily real because its existence is only guaranteed over the complex numbers.

Remeshing in P^4. To remesh a triangle mesh in P^4 into a PQ-mesh we first choose the affine chart $\mathbb{R}^4$ by de-homogenizing with $x_5 = 1$ and thus having spheres represented as in (2). Conjugate parametrizations are invariant under projective maps (as they are planarity preserving). Consequently, projecting the mesh vertices $\mathbf{v} = (x_1, x_2, x_3, x_4)$ into meshes in $\mathbb{R}^3$ by leaving out coordinates keeps the property of a conjugate net: $\mathbf{v}' = (x_1, x_2, x_3)$ and $\mathbf{v}'' = (x_1, x_2, x_4)$ or in terms of the sphere congruence that is

$$\tilde{\mathbf{s}}' = \frac{2(c_1, c_2, c_3)}{\mathbf{c}^2 - r^2 + 1} \quad \text{and} \quad \tilde{\mathbf{s}}'' = \frac{(2c_1, 2c_2, \mathbf{c}^2 - r^2 - 1)}{\mathbf{c}^2 - r^2 + 1}.$$

If we find a parametrization of $\tilde{\mathbf{s}}$ that is simultaneously conjugate for $\tilde{\mathbf{s}}'$ and $\tilde{\mathbf{s}}''$, it must also be conjugate for $\tilde{\mathbf{s}}$: The existence of functions a, b, A, B with $\tilde{\mathbf{s}}'_{uv} = a\tilde{\mathbf{s}}'_u + b\tilde{\mathbf{s}}'_v$ and $\tilde{\mathbf{s}}''_{uv} = A\tilde{\mathbf{s}}''_u + B\tilde{\mathbf{s}}''_v$ yields $a = A$ and $b = B$ and thus $\tilde{\mathbf{s}}_{uv} = a\tilde{\mathbf{s}}_u + b\tilde{\mathbf{s}}_v$. This shows that $\tilde{\mathbf{s}}$ is a conjugate parametrization. We have

Proposition 6.2. *A generic parametrization $\tilde{\mathbf{s}} : \mathbb{R}^2 \to \mathbb{R}^4$ is conjugate if and only if its two projections $\tilde{\mathbf{s}}'$ and $\tilde{\mathbf{s}}''$ are conjugate.*

Thus, to find the conjugate parametrization of $\tilde{\mathbf{s}}$ we must find tangent directions $\mathbf{t}, \bar{\mathbf{t}}$ which simultaneously solve $\mathbf{t} \cdot \mathrm{II}' \cdot \bar{\mathbf{t}} = 0$ and $\mathbf{t} \cdot \mathrm{II}'' \cdot \bar{\mathbf{t}} = 0$, where II' and II'' are the second fundamental forms of $\tilde{\mathbf{s}}'$, $\tilde{\mathbf{s}}''$, respectively. These directions are found as eigenvectors of

$$\mathrm{II}'^{-1} \cdot \mathrm{II}''. \tag{12}$$

In practice $\tilde{\mathbf{s}}', \tilde{\mathbf{s}}''$ are triangle meshes. We approximate II' and II'' through jet-fitting (cf. [Cazals and Pouget 2005]). In all our experiments the triangle meshes had a shape where the matrix (12) had *real* eigenvectors even though theoretically one can construct surface pairs $\tilde{\mathbf{s}}', \tilde{\mathbf{s}}''$ for which the eigenvectors are imaginary.

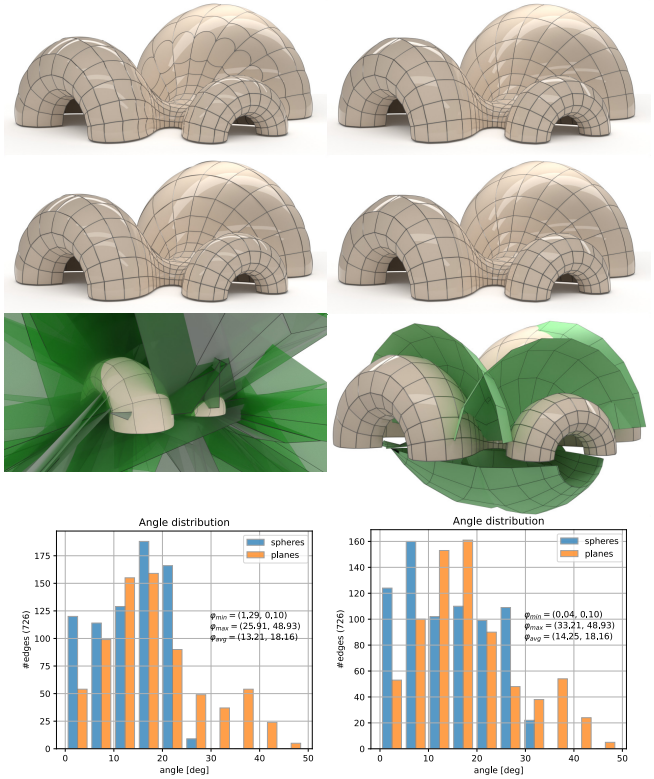

Fig. 28. Angle minimizing spheres paneling a circular mesh. *Left:* Just angle minimization. *Right:* Optimized for the additional constraint such that the intersection circle of neighboring spheres lies in the bisecting plane of the corresponding faces. *Top-Row:* Edges/beams as exact intersection circles. *Second-Row:* Edges/beams in bisecting planes. *Third-Row-Left:* The mesh of centers of the face spheres is depicted in green. Note that there is no constraint imposed on the centers resulting in a very chaotic mesh compared to the one on the (*right*). *Third-Row-Right:* The mesh of centers of the face spheres is depicted in green. Note that this green mesh is by construction in a sense a parallel mesh. *Bottom-Row:* Histogram of intersection angles. The values of the spherical panelization (in blue) compared to the values of the paneling with planar faces (in orange) are much smaller.

In the case of real conjugate directions we apply the remeshing algorithm by [Panozzo et al. 2014] to $\tilde{\mathbf{s}}''$. We could also apply remeshing to $\tilde{\mathbf{s}}'$, but in all our experiments the surface $\tilde{\mathbf{s}}''$ turned out to be the smoother and more regularly parametrized mesh.

We obtain an "almost" PQ-mesh in $\mathbb{R}^4$ by mapping the remeshed quad mesh back from $\tilde{\mathbf{s}}''$ to $\tilde{\mathbf{s}}$. We finally apply a post-optimization step to planarize the faces of the new mesh in P^4 using the method of [Tang et al. 2014]. A planar face in $\mathbb{R}^4$ is characterized by two orthogonal unit normal vectors that are perpendicular to all edges of that face. This quad mesh represents the face spheres of an SQ-mesh with support structure enveloping the same surface as the given sphere congruence. See Figure 29 for an example.

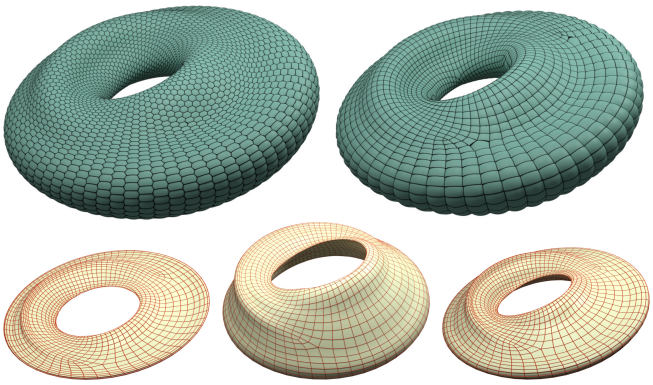

Fig. 29. Remeshing of a sphere congruence. *Top-Left:* A given SHex-mesh torus. *Top-Right:* SQ-remeshing of the SHex-mesh. *Bottom-Left and Center:* The projections of the mesh in P^4 to the first three coordinates $\mathbf{v}' = (x_1, x_2, x_3)$ (*left*) and projection to $\mathbf{v}'' = (x_1, x_2, x_4)$ (*center*). *Bottom-Right:* PQ-mesh of sphere centers after post optimization for planarity.

7 HEXAGONAL SPHERE MESHES

The mesh of sphere centers of a trivalent sphere mesh (in particular an SHex-mesh) is a triangle mesh and therefore always polyhedral. Therefore, SHex-meshes always have a geometric support structure. However, not every such support structure is really useful in a practical sense, since intersection circles of neighboring spheres might be contained in planes closer to the tangent plane than to normal planes which are more preferred. We will make use of an optimization strategy to ensure good solutions.

Our goal is to find an SHex-mesh approximating a given triangle mesh or smooth parametrization. A similar task is to approximate a given surface with planar hexagons. Ways to attack the latter problem, for example by intersecting tangent planes of the surface to obtain PHex-meshes have been described in [Pluta et al. 2021; Troche 2008; Zimmer et al. 2013] also pointing out the many difficulties arising there and suggesting solutions. However we have more degrees of freedom when intersecting spheres instead of planes. We get the following two insights from the PHex case: (i) positively curved surfaces are generically covered by convex hexagons and (ii) negatively curved surfaces are generically covered by bow-tie shaped hexagons.

The Gaussian curvature K is not Möbius invariant, not even its sign. Away from an umbilical point there is always a Möbius transformation that can locally change a positively curved region into a negatively curved region and vice versa. For example by mapping the central sphere to a plane the surface region becomes negatively curved. Or by mapping a sufficiently small tangential sphere (which does not intersect the surface locally) to a plane generates a positively curved surface region. In theory we could perform this curvature change if necessary and locally intersect tangent planes and transform back.

From this observation we conclude that both, positively as well as negatively curved surfaces

should be coverable with both types of spherical faces, convex and bow-tie shapes, respectively. By convex and bow-tie faces we refer to spherical polygons which are Möbius equivalent to planar convex or bow-tie hexagons.

Spherical hexagons appearing convex. Spherical hexagons can look rather complicated (crisscrossed) or degenerated. However, those spherical hexagons which appear in practice have a convex hull that is fairly two-dimensional. When looking at such a spherical hexagon orthogonally to its two-dimensional extent, they only mildly deviate from a planar hexagonal polygon, see Figure 30.

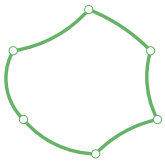

Fig. 30. Orthogonal projection of a spherical hexagon along the direction of its in size largest shadow. Projecting hexagons which appear in practice in this way will only mildly deviate from planar hexagonal polygons. We call the *left* hexagon *visually convex* and the *right* one *visually bow-tie shaped.*

Vaguely speaking, we visually identify the spherical hexagon with a planar hexagonal polygon. In this sense we can speak of a *visually convex* spherical hexagon if its close by planar hexagonal polygon is convex. Analogously, we refer to *visually bow-tie shaped* spherical hexagons.

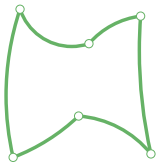

Whenever we want to cover a surface with visually convex spherical hexagons we take the positively curved PHex-case as a prototype. The corresponding planes are tangent planes which locally do not intersect the surface. Consequently, to achieve a sphere mesh of that sort we will intersect spheres $s_\emptyset$ tangential to the surface which locally do not intersect that surface.

Whether a tangent sphere locally intersects the surface (like a tangent plane in a negatively curved surface point) depends on where it lies in the parabolic pencil of all touching spheres (see Figure 31). The parabolic sphere pencil is represented by a projective line in P^4 which – topologically speaking – is a circle (see Figure 31).

Sufficiently small spheres $s_\emptyset$ in this pencil locally do not intersect the surface. The "first" spheres that intersect the surface are the principal curvature spheres. The central sphere always intersects

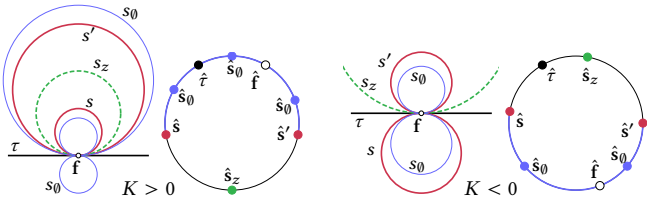

Fig. 31. The parabolic pencil of tangent spheres contains the surface point $\mathbf{f}$, the tangent plane τ, the two curvature spheres s, s' (red), and the central sphere s_z (green). In the projective model of Möbius geometry the sphere pencil is represented by the points of a projective line which is topologically a circle, split into two segments by the curvature spheres. On this circle $\hat{\mathbf{s}}_z$ and $\hat{\mathbf{f}}$ lie in different segments. The spheres $s_\emptyset$ of the pencil which locally do not intersect the surface (blue) lie in the same segment as the point.

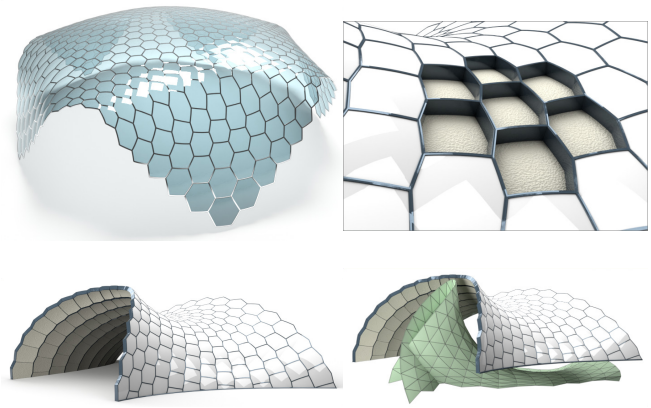

Fig. 32. SHex-meshes with support structures from intersecting tangential spheres. *Top-Left:* An SHex-mesh paneling with visually convex hexagons. However note that these hexagons are not planar and the classical notion of convexity does not apply here. *Bottom-Left:* An SHex-mesh paneling a negatively curved surface. Again, the spherical hexagonal faces give the impression of convex hexagons which is only possible because the faces are proper spheres. Planar faces paneling a negatively curved region would result in bow-tie shaped hexagons. *Top-Right:* These meshes posses a geometric support structure as illustrated on a detail of the bottom-left SHex-mesh. *Bottom-Right:* The vertices of the green mesh are the centers of the spheres. Note that the combinatorics of the mesh of centers which is the same as the combinatorics of the mesh of spheres in P^4 is dual to the sphere mesh.

the surface. Thus, to obtain visually convex shaped spherical faces after intersecting neighboring spheres we choose spheres $s_\emptyset$ among those which locally do not intersect the surface (blue in Figure 31).

We want our face spheres to be as close as possible to the curvature spheres, since those approximate the surface better than small spheres. To achieve both goals, obtaining large enough spheres and avoiding the "forbidden area", our optimization approach is initialized with a choice of small enough spheres and then evolves towards the closest principal curvature spheres.

We accomplish this evolution by fixing a triangle mesh on the surface and initialize a congruence of spheres of equal and sufficiently small radius. The centers thus lie on a close enough offset surface. The evolution now brings the centers of these spheres closer to the curvature centers. Recall that the node axis at a vertex is orthogonal to the corresponding face of sphere centers. To obtain a good support structure we require this node axis not to exceed a prescribed angle with the corresponding face normal of the fixed triangle mesh.

See Fig. 32 for examples where positively and negatively curved surface areas have been paneled with visually convex spherical hexagons. For negatively curved surfaces this effect could not have been achieved by a PHex-mesh.

A similar strategy as in the visually convex spherical hexagons case can be used to obtain visually bow-tie shaped spherical faces even in positively curved surface regions. This time we require the spheres to lie between the principal spheres on the same side as the central sphere (see Fig. 31). Otherwise the strategy is the same. Visually bow-tie shaped spherical hexagons in positively curved regions also appear in the bottom row of Fig. 17. Also here the typical difficulties arise, as pointed out by [Zimmer et al. 2013] in the case of intersecting tangent planes. These include self-intersecting face edges, extreme variations in edge lengths or uneven distribution of angles between edges.

Generating hexagonal sphere meshes. After choosing a triangulation $M = (V, E, F)$ of the surface to be approximated we start with congruent spheres which touch the given surface in the vertices $\mathbf{v}_i \in V$ of the triangulation. Its centers $\mathbf{c}_i$ are chosen on one side of the surface and thus constitute a discrete offset: $\mathbf{c}_i = \mathbf{v}_i + \lambda_i \mathbf{n}_i$ where $\mathbf{n}_i$ is the unit normal vector at $\mathbf{v}_i$. At first λ_i is constant. To bring the spheres closer to one of the curvature spheres (whichever one is closer) we minimize

$$E_{\text{cs}} = \sum_i |\lambda_i - \rho_i|^2,$$

where ρ_i denotes the smaller principal curvature radius if $K > 0$ or the only principal curvature radius if $K < 0$. We exclude here surfaces where different regions with positive K have curvature centers on different sides of the surface; keeping the sphere centers on one side would result in "spiky" surfaces as in Fig. 26 (b) and 27.

Additionally we want to keep the intersection circle of neighboring spheres in planes nearly orthogonal to the surface. For that we minimize for every combinatorial triangle $t = ijk$ the angle between the unit normal vector $\mathbf{n}_c^t$ of $\mathbf{c}_i\mathbf{c}_j\mathbf{c}_k$ and $\mathbf{n}_v^t = (\mathbf{n}_i + \mathbf{n}_j + \mathbf{n}_k)/3$:

$$E_{\text{ortho}} = \sum_{t \in F} \|\langle \mathbf{n}_c^t, \mathbf{n}_v^t \rangle^2 - \delta^2 - \mu_t^2\|^2,$$

where δ denotes the chosen angle threshold and where μ_t introduce "slack variables" to transform the inequality into an equation. A regularizing Laplacian smoothing term E_{fair} applied to the mesh of centers ensures a fair arrangement. Our optimization is using the Levenberg-Marquardt algorithm [Marquardt 1963]. Smooth sphere congruences resulting from this method can also be used as an input to be remeshed into an SQ-mesh (Sec. 6.4).

8 CONCLUSION

Limitations. A systematic study of meshes with spherical faces is a new topic, and thus we could not aim at completeness in this contribution. To give examples: We showed how to obtain smoother skins with spherical panels than with planar ones, but we are lacking good criteria on a given shape whether the use of spherical panels will provide a clear advantage. Also, we did not address the problem of self-intersections in hexagonal panels when working with the bow-tie type.

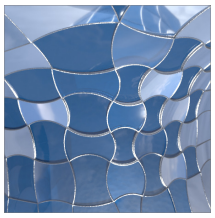

Without optimizing for a support structure the intersection circles of neighboring spheres can lie in very tangential positions. This results in edges that might not be usable as statically stable support structure, but can still result in nice patterns and is a design variant that needs further investigation.

Furthermore, the remeshing with SQ-meshes can lead to visually non-pleasing results and is a direction for further research.

Conclusion. We presented a study of meshes with spherical faces within Möbius geometry that has been motivated by applications in architecture, but is expected to have impact beyond that. Our

focus has been on the relation to surface paneling and to sphere congruences and their envelopes. We addressed the important case where one envelope is a given design surface and the congruence has to be computed in view of the application (hexagonal panels, as smooth as possible skins, existence of a support structure). The length of our paper also arises from our aim to make it accessible to non-experts in sphere geometries.

Future research. While we hope to have made a substantial initial contribution, the problem area is still wide open. Future work within the setting of Möbius geometry includes the topics addressed under limitations. We did not consider structural properties of support structures, which raises the question whether the increased flexibility in having spherical rather than flat quad panels with a support structure provides enough degrees of freedom to better align it with principal stress directions. We have already started to work within the other classical sphere geometries, namely the ones of Laguerre and Lie. One obtains, for example, smooth skins whose panels are spherical or parts of Dupin cyclides, arranged in a checkerboard pattern. Most likely, such structures provide an advantage for discrete differential sphere geometry, which is a largely unexplored area.

ACKNOWLEDGMENTS

The authors gratefully acknowledge the support by the SFB-Transregio "Discretization in Geometry and Dynamics" through grant I 2978 of the Austrian Science Fund (FWF) as well as by project F77 (SFB "Advanced Computational Design") and by KAUST baseline funding. Furthermore, the authors would like to thank the anonymous reviewers for their valuable comments.

REFERENCES

Oswin Aichholzer, Wolfgang Aigner, Franz Aurenhammer, Kateřina Čech Dobiášová, Bert Jüttler, and Günter Rote. 2015. Triangulations with Circular Arcs. *Journal of Graph Algorithms and Applications* 19, 1 (2015), 43–65. https://doi.org/10.7155/jgaa.00346

Wilhelm Blaschke. 1929. *Vorlesungen über Differentialgeometrie und geometrische Grundlagen von Einsteins Relativitätstheorie. Band III. Differentialgeometrie der Kreise und Kugeln.* Springer, Berlin.

Wilhelm Blaschke and Kurt Leichtweiß. 1973. *Elementare Differentialgeometrie.* Springer, Berlin-New York. Fünfte vollständig neubearbeitete Auflage von K. Leichtweiß, Die Grundlehren der mathematischen Wissenschaften, Band 1.

Pengbo Bo, Helmut Pottmann, Martin Kilian, Wenping Wang, and Johannes Wallner. 2011. Circular Arc Structures. *ACM Trans. Graph.* 30, 4 (2011), 101:1–101:11.

Alexander Bobenko and Yuri Suris. 2006. Isothermic surfaces in sphere geometries as Moutard nets. *Proceedings of The Royal Society A Mathematical Physical and Engineering Sciences* 463 (2006), 3171–3193.

Alexander I. Bobenko and Emanuel Huhnen-Venedey. 2012. Curvature line parametrized surfaces and orthogonal coordinate systems: discretization with Dupin cyclides. *Geom. Dedicata* 159 (2012), 207–237.

Alexander I. Bobenko, Helmut Pottmann, and Johannes Wallner. 2010. A curvature theory for discrete surfaces based on mesh parallelity. *Math. Ann.* 348, 1 (2010), 1–24.

Alexander I. Bobenko and Peter Schröder. 2005. Discrete Willmore Flow. In *Proc. Eurographics Symposium on Geometry Processing*. Eurographics Assoc., 101–110.

Alexander I. Bobenko and Yury B. Suris. 2007. On organizing principles of discrete differential geometry. Geometry of spheres. *Russian Mathematical Surveys* 62, 1 (2007), 1–43.

Alexander I. Bobenko and Yuri B. Suris. 2008. *Discrete differential geometry. Integrable structure.* Graduate Studies in Mathematics, Vol. 98. American Mathematical Society.

Frederic Cazals and Marc Pouget. 2005. Estimating differential quantities using polynomial fitting of osculating jets. *Computer Aided Geometric Design* 22, 2 (2005), 121–146.

Ho-Lun Cheng and Xinwei Shi. 2005. Quality Mesh Generation for Molecular Skin Surfaces Using Restricted Union of Balls. In *16th IEEE Visualization Conference, Proceedings.* IEEE Computer Society, 399–405.

Ho-Lun Cheng, Tamal K. Dey, Herbert Edelsbrunner, and John Sullivan. 2001. Dynamic Skin Triangulation. *Discrete Comput. Geom.* 25, 4 (2001), 525–568.

Keenan Crane, Ulrich Pinkall, and Peter Schröder. 2013. Robust Fairing via Conformal Curvature Flow. *ACM Trans. Graph.* 32 (2013). Issue 4.

Herbert Edelsbrunner. 1993. The Union of Balls and Its Dual Shape. In *Proceedings of the Ninth Annual Symposium on Computational Geometry (SCG '93).* Association for Computing Machinery, 218–231.

Herbert Edelsbrunner. 1999. Deformable smooth surface design. *Discrete Comput. Geom.* 21 (1999), 87–115.

Herbert Edelsbrunner and John L. Harer. 2010. *Computational Topology: An Introduction.* American Math. Soc.

Herbert Edelsbrunner and Ernst P. Mücke. 1994. Three-Dimensional Alpha Shapes. 13, 1 (1994), 43–72.

Michael Eigensatz, Martin Kilian, Alexander Schiftner, Niloy J. Mitra, Helmut Pottmann, and Mark Pauly. 2010. Paneling Architectural Freeform Surfaces. *ACM Trans. Graph.* 29, 4 (2010), 45:1–45:10.

Luther Pfahler Eisenhart. 1962. *Transformations of surfaces* (second ed.). Chelsea Publishing Co., New York. xi+379 pages.

Gaël Guennebaud and Markus Gross. 2007. Algebraic Point Set Surfaces. *ACM Trans. Graph.* 26, 3 (2007), 10.

Udo Hertrich-Jeromin. 2003. *Introduction to Möbius Differential Geometry.* Cambridge University Press.

Elias Jadon, Bernhard Thomaszewski, Aleksandra Anna Apolinarska, and Roi Poranne. 2022. Continuous Deformation Based Panelization for Design Rationalization. *ACM Transaction on Graphics (Proc. SIGGRAPH Asia 2022)*, Article 44 (2022), 8 pages.

Caigui Jiang, Hui Wang, Victor Ceballos Inza, Felix Dellinger, Florian Rist, Johannes Wallner, and Helmut Pottmann. 2021. Using isometries for computational design and fabrication. *ACM Trans. Graphics* 40, 4 (2021), 42:1–42:12. Proc. SIGGRAPH.

Felix Klein. 1968. *Vorlesungen über nicht-euklidische Geometrie.* Springer-Verlag, Berlin. xii+326 pages.

Daoming Liu, Davide Pellis, Yu-Chou Chiang, Florian Rist, Johannes Wallner, and Helmut Pottmann. 2023. Deployable strip structures. *ACM Trans. Graphics* 42, 4 (2023), xx:1–xx:16. Proc. SIGGRAPH.

Yang Liu, Helmut Pottmann, Johannes Wallner, Yong-Liang Yang, and Wenping Wang. 2006. Geometric modeling with conical meshes and developable surfaces. *ACM Trans. Graphics* 25, 3 (2006), 681–689. Proc. SIGGRAPH.

Donald W. Marquardt. 1963. An Algorithm for Least-Squares Estimation of Nonlinear Parameters. *J. Soc. Indust. Appl. Math.* 11, 2 (1963), 431–441.

Daniele Panozzo, Enrico Puppo, Marco Tarini, and Olga Sorkine-Hornung. 2014. Frame Fields: Anisotropic and Non-Orthogonal Cross Fields. *ACM Transactions on Graphics (proceedings of ACM SIGGRAPH)* 33, 4 (2014), 134:1–134:11.

Davide Pellis, Martin Kilian, Felix Dellinger, Johannes Wallner, and Helmut Pottmann. 2019. Visual smoothness of polyhedral surfaces. *ACM Trans. Graphics* 38, 4 (2019), 260:1–260:11. Proc. SIGGRAPH.

Davide Pellis, Martin Kilian, Helmut Pottmann, and Mark Pauly. 2021. Computational design of Weingarten surfaces. *ACM Trans. Graphics* 40, 4 (2021), 114:1–114:11.

Davide Pellis, Hui Wang, Martin Kilian, Florian Rist, Helmut Pottmann, and Christian Müller. 2020. Principal symmetric meshes. *ACM Trans. Graphics* 39, 4 (2020), 127:1–127:17. Proc. SIGGRAPH.

Kacper Pluta, Michal Edelstein, Amir Vaxman, and Mirela Ben-Chen. 2021. PH-CPF: Planar Hexagonal Meshing Using Coordinate Power Fields. *ACM Trans. Graph.* 40, 4, Article 156 (2021), 19 pages.

Helmut Pottmann, Michael Eigensatz, Amir Vaxman, and Johannes Wallner. 2015. Architectural Geometry. *Computers and Graphics* 47 (2015), 145–164.

Helmut Pottmann and Martin Peternell. 2000. Envelopes – Computational Theory and Applications. In *Spring Conference on Computer Graphics 2000*, B. Falcidieno (Ed.). Comenius University, Bratislava, 3–23. Proceedings of the conference in Budmerice, May 3-6, 2000.

Thilo Rörig and Gudrun Szewieczek. 2021. The Ribaucour families of discrete R-congruences. *Geom. Dedicata* 214 (2021), 251–275.

Yousuf Soliman, Albert Chern, Olga Diamanti, Felix Knöppel, Ulrich Pinkall, and Peter Schröder. 2021. Constrained Willmore Surfaces. *ACM Trans. Graph.* 40, 4, Article 112 (2021), 17 pages.

Chengcheng Tang, Xiang Sun, Alexandra Gomes, Johannes Wallner, and Helmut Pottmann. 2014. Form-finding with Polyhedral Meshes Made Simple. *ACM Trans. Graph.* 33, 4 (2014), 70:1–70:9.

Jean-Marc Thiery, Emilie Guy, and Tamy Boubekeur. 2013. Sphere-Meshes: Shape Approximation using Spherical Quadric Error Metrics. *ACM Transaction on Graphics (Proc. SIGGRAPH Asia 2013)* 32, 6 (2013), 178:1–178:12.

Jean-Marc Thiery, Émilie Guy, Tamy Boubekeur, and Elmar Eisemann. 2016. Animated Mesh Approximation With Sphere-Meshes. *ACM Trans. Graph.* 35, 3 (2016), 30:1–30:13.

Anastasia Tkach, Mark Pauly, and Andrea Tagliasacchi. 2016. Sphere-Meshes for Real-Time Hand Modeling and Tracking. *ACM Trans. Graph.* 35, 6 (2016), 222:1–222:11.

Christian Troche. 2008. Planar hexagonal meshes by tangent plane intersection. *Advances in Architectural Geometry* 1 (01 2008), 57–60.

Amir Vaxman, Christian Müller, and Ofir Weber. 2015. Conformal Mesh Deformations with Möbius Transformations. *ACM Trans. Graph.* 33, 4 (2015), 55:1–55:11.
Amir Vaxman, Christian Müller, and Ofir Weber. 2018. Canonical Möbius Subdivision. *ACM Trans. Graph.* 37, 6 (2018), 227:1–227:15.
Hui Wang, Davide Pellis, Florian Rist, Helmut Pottmann, and Christian Müller. 2019. Discrete geodesic parallel coordinates. *ACM Trans. Graph.* 38, 6 (2019), 173:1–173:13.
Henrik Zimmer, Marcel Campen, Ralf Herkrath, and Leif Kobbelt. 2013. Variational Tangent Plane Intersection for Planar Polygonal Meshing. In *Advances in Architectural Geometry 2012*, Lars Hesselgren et al. (Ed.). Springer Vienna, Vienna, 319–332.

A APPENDIX

A.1 Proof of Lemma 2.1

Proof. A sphere congruence has two real envelopes if and only if the intersection line of the two planes

$$\partial_u S(u,v,\mathbf{x}) = 0, \quad \text{and} \quad \partial_v S(u,v,\mathbf{x}) = 0.$$

intersects the sphere $S(u,v,\mathbf{x}) = 0$ in two real points. This is the case if and only if the distance of this line is closer to the center $\mathbf{c}$ of the sphere than its radius r.

The distance of the intersection line to $\mathbf{c}$ equals the diameter of the circumcircle of $\mathbf{c}$, $\mathbf{a} := \mathbf{c} - \frac{r r_u}{\|\mathbf{c}_u\|^2}\mathbf{c}_u$ and $\mathbf{b} := \mathbf{c} - \frac{r r_v}{\|\mathbf{c}_v\|^2}\mathbf{c}_v$, which is

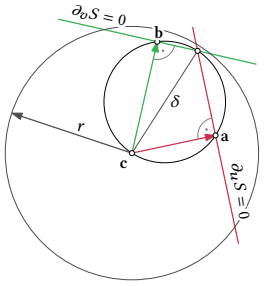

$$\delta := \frac{\|\mathbf{a}-\mathbf{b}\|}{\sin\angle(\mathbf{a}-\mathbf{c},\mathbf{b}-\mathbf{c})} = \frac{\left\|\frac{r r_u}{\|\mathbf{c}_u\|^2}\mathbf{c}_u - \frac{r r_v}{\|\mathbf{c}_v\|^2}\mathbf{c}_v\right\|}{\sin\angle(\mathbf{c}_u,\mathbf{c}_v)}.$$

Consequently, there are two real envelopes if and only if $\delta < r$ or squared

$$\left\|\frac{r_u}{\|\mathbf{c}_u\|^2}\mathbf{c}_u - \frac{r_v}{\|\mathbf{c}_v\|^2}\mathbf{c}_v\right\|^2 < 1 - \cos^2\angle(\mathbf{c}_u,\mathbf{c}_v) = 1 - \frac{\langle \mathbf{c}_u,\mathbf{c}_v\rangle^2}{\|\mathbf{c}_u\|^2\|\mathbf{c}_v\|^2},$$

which is further equivalent to

$$\left\|r_u\|\mathbf{c}_v\|\frac{\mathbf{c}_u}{\|\mathbf{c}_u\|} - r_v\|\mathbf{c}_u\|\frac{\mathbf{c}_v}{\|\mathbf{c}_v\|}\right\|^2 < \|\mathbf{c}_u\|^2\|\mathbf{c}_v\|^2 - \langle \mathbf{c}_u,\mathbf{c}_v\rangle^2.$$

Exploiting the identity $\|\lambda\mathbf{p} + \mu\mathbf{q}\| = \|\mu\mathbf{p} + \lambda\mathbf{q}\|$ for vectors $\mathbf{p},\mathbf{q}$ with $\|\mathbf{p}\| = \|\mathbf{q}\|$ the above condition simplifies to

$$\|r_u\mathbf{c}_v - r_v\mathbf{c}_u\|^2 < \|\mathbf{c}_u\|^2\|\mathbf{c}_v\|^2 - \langle \mathbf{c}_u,\mathbf{c}_v\rangle^2. \qquad \square$$

A.2 Proof of Lemma 6.1

Proof. We must show that $\hat{\mathbf{s}}_{ik}$ bisects the angle formed by the two spheres $\hat{\mathbf{s}}_i$ and $\hat{\mathbf{s}}_k$ in its acute angle. We have

$$\langle\!\langle \hat{\mathbf{s}}_i, \hat{\mathbf{s}}_k\rangle\!\rangle = 2(r_i^2 + r_k^2 - \|\mathbf{c}_i - \mathbf{c}_k\|^2)$$

and consequently $\langle\!\langle \hat{\mathbf{s}}_i, \hat{\mathbf{s}}_i\rangle\!\rangle = 4r_i^2$ and $\langle\!\langle \hat{\mathbf{s}}_k, \hat{\mathbf{s}}_k\rangle\!\rangle = 4r_k^2$. Using

$$\langle\!\langle \hat{\mathbf{s}}_i, \hat{\mathbf{s}}_{ik}\rangle\!\rangle = \langle\!\langle \hat{\mathbf{s}}_i, \varepsilon r_k\hat{\mathbf{s}}_i + r_i\hat{\mathbf{s}}_k, \rangle\!\rangle = 4\varepsilon r_i^2 r_k + r_i\langle\!\langle \hat{\mathbf{s}}_i, \hat{\mathbf{s}}_k\rangle\!\rangle$$

and

$$\begin{aligned}\langle\!\langle \hat{\mathbf{s}}_{ik}, \hat{\mathbf{s}}_{ik}\rangle\!\rangle &= 4r_i^2r_k^2 + 2\varepsilon r_i r_k\langle\!\langle \mathbf{s}_i, \mathbf{s}_k\rangle\!\rangle + 4r_i^2r_k^2 \\ &= 2r_i r_k(4r_i r_k + |\langle\!\langle \hat{\mathbf{s}}_i, \hat{\mathbf{s}}_k\rangle\!\rangle|),\end{aligned}$$

the cosine of the angle between the spheres represented by $\hat{\mathbf{s}}_i$ and $\hat{\mathbf{s}}_{ik}$ equals

$$|\cos\angle(\hat{\mathbf{s}}_i, \hat{\mathbf{s}}_{ik})| = \frac{4r_i r_k + |\langle\!\langle \hat{\mathbf{s}}_i, \hat{\mathbf{s}}_k\rangle\!\rangle|}{\sqrt{2}\sqrt{(4r_i r_k)^2 + 4r_i r_k|\langle\!\langle \hat{\mathbf{s}}_i, \hat{\mathbf{s}}_k\rangle\!\rangle|}}$$

and analogously

$$|\cos\angle(\hat{\mathbf{s}}_k, \hat{\mathbf{s}}_{ik})| = \frac{4r_i r_k + |\langle\!\langle \hat{\mathbf{s}}_i, \hat{\mathbf{s}}_k\rangle\!\rangle|}{\sqrt{2}\sqrt{(4r_i r_k)^2 + 4r_i r_k|\langle\!\langle \hat{\mathbf{s}}_i, \hat{\mathbf{s}}_k\rangle\!\rangle|}}.$$

It follows that the cosine of the angles might only differ by the sign implying that either

$$\angle(\hat{\mathbf{s}}_i, \hat{\mathbf{s}}_{ik}) = \angle(\hat{\mathbf{s}}_k, \hat{\mathbf{s}}_{ik}) \quad \text{or} \quad \angle(\hat{\mathbf{s}}_i, \hat{\mathbf{s}}_{ik}) = \pi - \angle(\hat{\mathbf{s}}_k, \hat{\mathbf{s}}_{ik}).$$

Consequently, the sphere represented by $\hat{\mathbf{s}}_{ik}$ (and angalogously $\hat{\mathbf{s}}_o$) bisects the two spheres $\hat{\mathbf{s}}_i$ and $\hat{\mathbf{s}}_k$. To see that $\hat{\mathbf{s}}_{ik}$ lies in its acute angle we compute

$$\begin{aligned}|\cos\angle(\hat{\mathbf{s}}_i, \hat{\mathbf{s}}_{ik})| &= \frac{4r_i r_k + |\langle\!\langle \hat{\mathbf{s}}_i, \hat{\mathbf{s}}_k\rangle\!\rangle|}{\sqrt{2}\sqrt{(4r_i r_k)^2 + 4r_i r_k|\langle\!\langle \hat{\mathbf{s}}_i, \hat{\mathbf{s}}_k\rangle\!\rangle|}} \\ &= \frac{4r_i r_k + |\langle\!\langle \hat{\mathbf{s}}_i, \hat{\mathbf{s}}_k\rangle\!\rangle|}{\sqrt{2}\sqrt{(4r_i r_k + |\langle\!\langle \hat{\mathbf{s}}_i, \hat{\mathbf{s}}_k\rangle\!\rangle|)^2 - 4r_i r_k|\langle\!\langle \hat{\mathbf{s}}_i, \hat{\mathbf{s}}_k\rangle\!\rangle| - |\langle\!\langle \hat{\mathbf{s}}_i, \hat{\mathbf{s}}_k\rangle\!\rangle|^2}} \\ &> \frac{4r_i r_k + |\langle\!\langle \hat{\mathbf{s}}_i, \hat{\mathbf{s}}_k\rangle\!\rangle|}{\sqrt{2}\sqrt{(4r_i r_k + |\langle\!\langle \hat{\mathbf{s}}_i, \hat{\mathbf{s}}_k\rangle\!\rangle|)^2}} = \frac{1}{\sqrt{2}},\end{aligned}$$

and conclude $\angle(\hat{\mathbf{s}}_i, \hat{\mathbf{s}}_{ik}) < \frac{\pi}{4}$ or $\pi - \angle(\hat{\mathbf{s}}_i, \hat{\mathbf{s}}_{ik}) < \frac{\pi}{4}$. $\square$

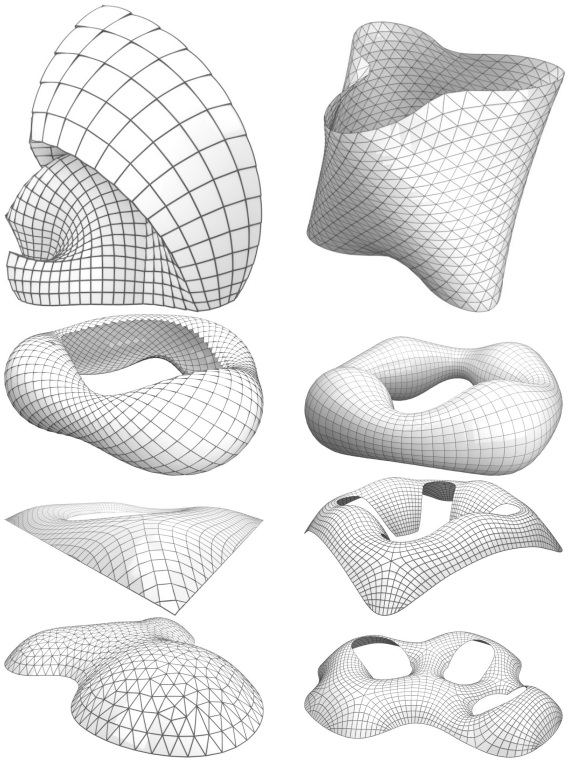

Fig. 33. Sphere meshes. The smaller the faces (typically triangles) become the less curvature must be covered by spherical faces resulting in spheres which are almost planes.